MOTOR FLOW INSTABILITIES - Part 2

Intrinsic linear stability of the flow induced by wall injection

G. Casalis, F. Vuillot

ONERA Toulouse - 2, av. Ed. Belin BP 4025 - 31 055 Toulouse Cedex - FRANCE
ONERA - BP72 - 29 av. de la Div. Leclerc - F-92 322 Châtillon Cedex - FRANCE

casalis@onecert.fr, vuillotf@onera.f

RTO-AVT VKI Special Course on

INTERNAL AERODYNAMICS IN SOLID ROCKET PROPULSION

VKI Institut, 27-31 May, 2002

Paper presented at the RTO/VKI Special Course on "Internal Aerodynamics in Solid Rocket Propulsion",
held in Rhode-Saint-Genèse, Belgium, 27-31 May 2002, and published in RTO-EN-023.

Report Documentation Page	*Form Approved* *OMB No. 0704-0188*

Public reporting burden for the collection of information is estimated to average 1 hour per response, including the time for reviewing instructions, searching existing data sources, gathering and maintaining the data needed, and completing and reviewing the collection of information. Send comments regarding this burden estimate or any other aspect of this collection of information, including suggestions for reducing this burden, to Washington Headquarters Services, Directorate for Information Operations and Reports, 1215 Jefferson Davis Highway, Suite 1204, Arlington VA 22202-4302. Respondents should be aware that notwithstanding any other provision of law, no person shall be subject to a penalty for failing to comply with a collection of information if it does not display a currently valid OMB control number.

1. REPORT DATE **00 JAN 2004**	2. REPORT TYPE **N/A**	3. DATES COVERED **-**

4. TITLE AND SUBTITLE **Motor Flow Instabilities Part 2 Intrinsic Linear Stability of the Flow Induced by Wall Injection**	5a. CONTRACT NUMBER 5b. GRANT NUMBER 5c. PROGRAM ELEMENT NUMBER
6. AUTHOR(S)	5d. PROJECT NUMBER 5e. TASK NUMBER 5f. WORK UNIT NUMBER
7. PERFORMING ORGANIZATION NAME(S) AND ADDRESS(ES) **ONERA BP 72 92322 Châtillon Cedex FRANCE**	8. PERFORMING ORGANIZATION REPORT NUMBER
9. SPONSORING/MONITORING AGENCY NAME(S) AND ADDRESS(ES)	10. SPONSOR/MONITOR'S ACRONYM(S) 11. SPONSOR/MONITOR'S REPORT NUMBER(S)

12. DISTRIBUTION/AVAILABILITY STATEMENT
Approved for public release, distribution unlimited

13. SUPPLEMENTARY NOTES
See also ADM001656., The original document contains color images.

14. ABSTRACT

15. SUBJECT TERMS

16. SECURITY CLASSIFICATION OF:			17. LIMITATION OF ABSTRACT	18. NUMBER OF PAGES	19a. NAME OF RESPONSIBLE PERSON
a. REPORT **unclassified**	b. ABSTRACT **unclassified**	c. THIS PAGE **unclassified**	**UU**	**64**	

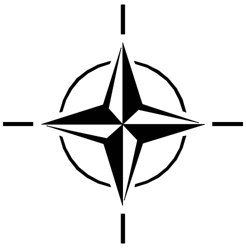

Contents

Introduction 5

1 Geometry, presentation 7
- 1.1 Experimental facilities 7
- 1.2 Notations 9
  - 1.2.1 Plane case 9
  - 1.2.2 Axisymmetric case 10
  - 1.2.3 Dimensionless quantities, Reynolds number 10
- 1.3 General equations 10
  - 1.3.1 Used assumptions 10
  - 1.3.2 Plane geometry 11
  - 1.3.3 Cylindrical geometry 12
- 1.4 Basic flow 12
  - 1.4.1 Plane case 12
  - 1.4.2 Axisymmetric case 13
  - 1.4.3 Some remarks 14

2 Linear Stability Theory 17
- 2.1 A short philosophical escape 17
- 2.2 Small perturbation technique 18
- 2.3 Normal mode form 19
- 2.4 Dispersion relation 20
- 2.5 Linearised equations 21
  - 2.5.1 Plane case 21
  - 2.5.2 Axisymmetric case 22

3 Stability results 25
- 3.1 Eigenmodes 25
- 3.2 Amplitude and n factor 26
  - 3.2.1 Definition of the n factor 26
  - 3.2.2 Plane case 28
  - 3.2.3 Axisymmetric case. 29
- 3.3 Influence of the Reynolds number 32
- 3.4 Comparisons with the experiment 33

- 3.4.1 Preparation of the results for the comparison 33
- 3.4.2 Effects of the dimensional height of the duct and injection velocity 34
- 3.4.3 Streamwise amplification 34

4 In(tro)spection of the used assumptions 41

- 4.1 Non parallel effects 41
  - 4.1.1 Definitions 41
  - 4.1.2 Use of a parallel approximation ? 42
  - 4.1.3 What is the matter with the normal non parallel approach ? 43
  - 4.1.4 Is there any consistent and accurate non parallel approach ? 45
- 4.2 Physical assumptions 47

Conclusion 49

ANNEX : Spectral collocation method 55

Introduction

Thrust oscillations generally occur in large solid propellant motor during a few seconds of the flight, they exactly correspond to the frequencies of the cavity modes. The excitation of cavity modes has been reproduced in small scale solid propellant motors and also in cold gas facilities. However as extensively exposed by F. Vuillot in the present VKI lecture series, there are different possible causes of this excitation and all of them may play a role. Among them, as suggested by F. Vuillot, see [1], there is the intrinsic instability.

Let us start with very simple models. Let be $\mathcal{L}(\omega)$ a linear differential operator for which some values of ω correspond to eigenmodes. It means that for these values, it exists a non zero solution $\hat{u}_\omega$ ($\hat{u}_\omega \not\equiv 0$) such as : $\mathcal{L}(\omega)(\hat{u}_\omega) = 0$. Now, ω is assumed to be such an eigenvalue and $\hat{u}_\omega$ the associated eigenfunction. If the system is forced by a non zero right hand side term f, we have to solve : $\mathcal{L}(\omega)(v) = f$. Thanks to the linear nature of the differential operator, if f may be decomposed in different terms $f = \sum f_i$, the solution v is the exact superposition of the solution of each isolated forcing $v = \sum v_i$ with $\mathcal{L}(\omega)(v_i) = f_i$. If f_i does not correspond to the eigenmode $\hat{u}_\omega$, the amplitude v_i remains as small as the one of the forcing f_i. On the other hand, if $f_{i,\omega}$ is an eigenmode (proportional to $\hat{u}_\omega$), then the amplitude of $v_{i,\omega}$ may become very large (it is the so-called secular terms in the framework of the multiple scale analysis, it is the so-called resonance phenomenon generally speaking). Consequently, after some transient, the contribution of $v_{i,\omega}$ in the sum $v = \sum v_i$ will be dominant, $v \approx v_{i,\omega}$: the system has selected a single behaviour, the one corresponding to the resonant forcing.

Coming back to the solid propellant motor, the previous operator $\mathcal{L}(\omega)$ may be associated to the governing problem for the cavity mode, the matter is to determine the origin of the forcing. An intrinsic instability mechanism has been suspected by François Vuillot to be responsible of the forcing. If it is the case, the forcing would be itself an eigenmode, but for another dynamical system !

The present course is limited to the presentation of the linear stability theory. We will show the general philosophy which is behind a so-called “instability”, the application of it for the special flow which is representative of the one in a solid propellant motor. We will also show that the present theory is very strange from a theoretical point of view, but very efficient in comparison with the available experimental results. Finally we will conclude as a “Public Prosecutor” against the intrinsic instability modes which are suspected to be the forcing terms with respect to the emergence of the dangerous cavity modes.

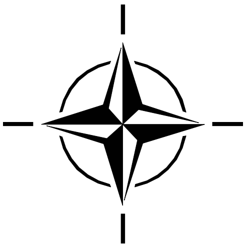

Chapter 1

Geometry, presentation

1.1 Experimental facilities

In real motors, the conditions are very severe (two-phase flow, high pressure, high temperature), so that detailed measurements inside the motor are nearly impossible. Cold gas experimental facilities have been thus especially designed for fundamental studies. They are much less expensive than the experiment which use solid propellant and detailed measurements are possible ; on the other hand some physical effects are missing such as the reactive two-phase flow or the slow regression of the wall (due to the combustion of the propellant).

For cold gas experiment, the flow inside the motor which comes from the burning surface in real motors is simulated by a wall injection of cold gas (air for example). This is usually realized by using a porous wall constituted by small bronze particles which are then compacted.

In the following, two types of geometry will be considered.

- The first one is of rectangular type. We will take benefit from only one facility of this kind :

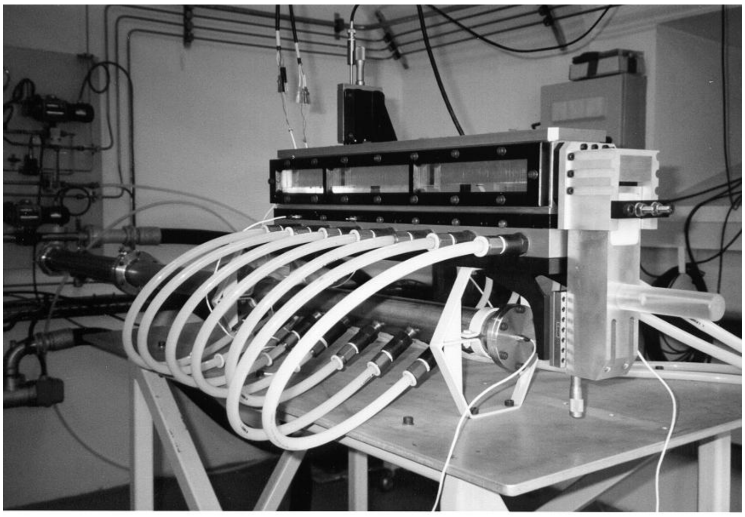

Figure 1.1: VECLA facility

the one called "VECLA", extensively studied by G. Avalon in ONERA Palaiseau, see [2] even if other facilities such as the so-called "Micat1" carried out in Poitiers, see [3], with which very interesting results have been obtained. A photo of VECLA is given in figure 1.1, whereas a sketch is given in figure 1.2. Its length and its breadth are fixed, 603 mm and 60 mm respectively.

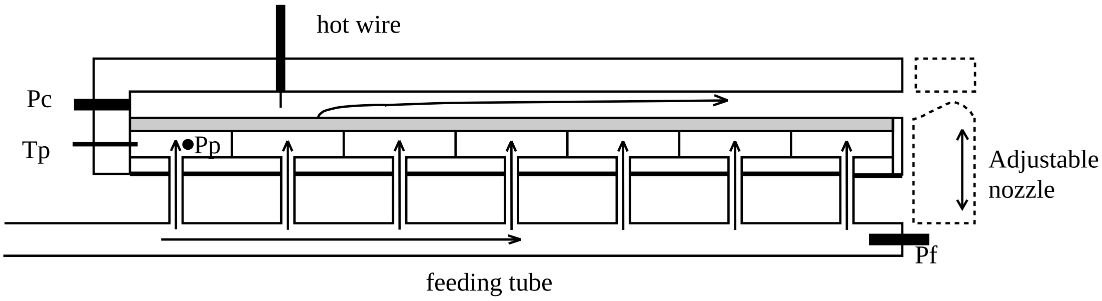

Figure 1.2: Sketch of the VECLA facility

On the other hand, the height can be modified, 10 mm, 20 mm and 30 mm have been tested. Air is injected only through the lower wall. The upper wall is solid and is perforated by small holes in order to maintain a hot wire anemometer used for measurement of the instantaneous velocity. The two lateral walls are in plexiglas allowing thus flow visualisations. In the theory presented in the following, we will considerer a plane case for which both lower and upper walls are used for the air injection. Finally the system is closed on one side by a front wall and ends on the other side by either nothing or by a non injecting nozzle leading to a throat. In the operating conditions, the flow is sonic at the throat. Without nozzle, the injection velocity may be varied continuously during the experience. It can also be fixed, typical values are around 1 m/s. The nozzle is adjustable, as indicated in figure 1.2, so that the injection velocity may be changed but not continuously during an experiment. In addition to some technical measurements necessary for the control of the flow, the measurements consist in the fluctuating pressure at the front wall (denoted by Pc in figure 1.2) and the velocity (mean value and fluctuating one) inside the flow by using a hot wire. This one can be moved at several distances from the front wall and different distances from the porous wall can be analysed. By using the so-called periodogram process, the temporal velocity signal is finally converted into a spectral representation. Very interesting and recent results obtained with VECLA may be found [4].

- The second geometry is closer than the one of real solid propellant motors, it is a cylinder. Results of different facilities will be used in the present document. The oldest one (whose results are used in the present document) is located in the United States and has been extensively tested by Brown and co-workers, see [5] for example. Another one is in Belgium and has been realized and studied by Jérome Anthoine, see [6], manager of the present lecture series ! Finally a more recent one is currently investigated at ONERA-Palaiseau by G. Avalon. A photo of this last facility is provided in figure 1.3. In that case, there is a unique cylindrical porous wall, through which cold gas is injected. The diameter is 60 mm. This case is obviously closer to the real geometry, but only one diameter can be used for a given system. As for the first geometry, there is a front wall and either a free exit section (as it is the case for the photo 1.3) or a

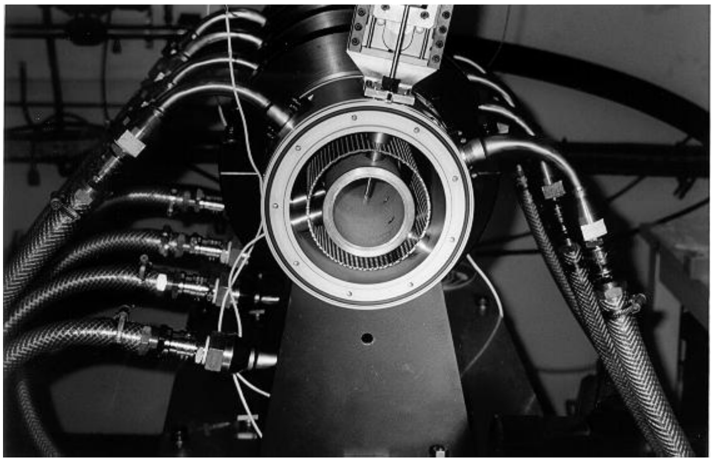

Figure 1.3: Photo of the VALDO facility

throat. As with VECLA, for a free exit section, the injection velocity can be varied more or less arbitrarily. Front wall pressure is measured and a hot wire is also used, it may be observed in photo 1.3. But for this type of installation with a hot wire passing through the porous wall, very few distances from the front wall can be analysed. In order to obtain finer experimental results for the evolution of the velocity with respect to the distance from the front wall, the hot wire has been installed on a very fine and long blade passing directly through the exit section.

1.2 Notations

1.2.1 Plane case

As sketched in figure 1.4, the x coordinate is defined in the direction perpendicular to the front wall, $x = 0$ being located at this wall. The coordinate denoted by y defines the distance from the upper and lower walls, $y = 0$ is located in the symmetry plane. Finally, the coordinate z defines the broadness. The distance between the upper and lower walls is denoted by $2h$, so that h is the physical distance between the two walls when considering the VECLA facility, for which the non porous wall is located at $y = 0$. The norm of the injection velocity through these walls is assumed

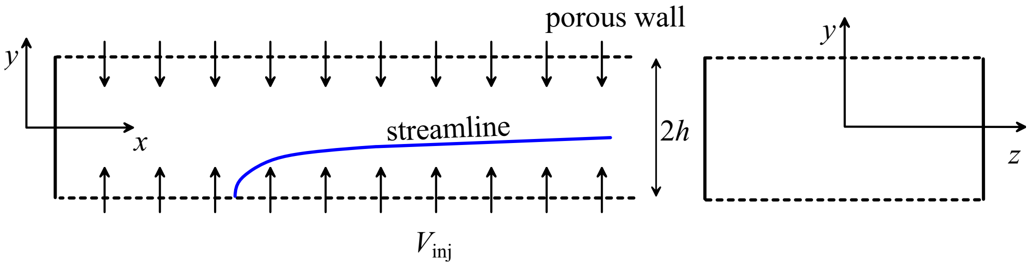

Figure 1.4: Plane notations

to be constant and uniform, it is noted V_{inj}.

1.2.2 Axisymmetric case

As in the first case, x represents the distance from the front wall. Otherwise, r denotes the radial coordinate and θ the azimuthal one. The geometry is sketched in figure 1.5. The diameter is noted by $2h$ and the norm of the injection velocity by V_{inj}, as for the plane case.

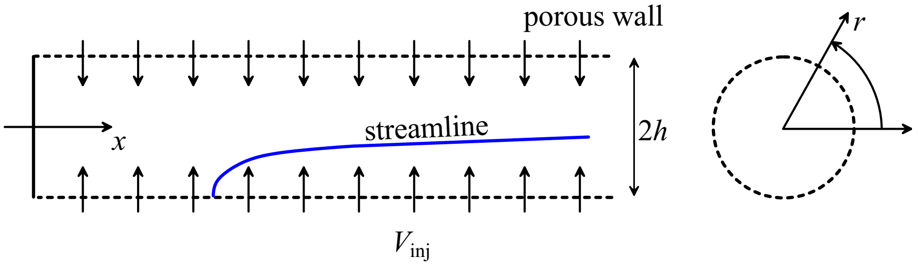

Figure 1.5: Axisymmetric notations

1.2.3 Dimensionless quantities, Reynolds number

In the following, all the quantities are dimensionless according to the reference velocity V_{inj} and the reference length h, it means that the lengths are scaled by the radius (and not by the diameter) of the cylinder in case of the axisymmetric geometry. The reference time is h/V_{inj} and the pressure is scaled with ρV_{inj}^2, ρ being the density (assumed to be constant). Thus, in the equations it appears a Reynolds number based on the injection velocity :

$$\mathcal{R} = \frac{hV_{\text{inj}}}{\nu}$$

where ν represents the kinematic viscosity. In the operating conditions, this Reynolds number is of order 1000. In some papers, like [7], another Reynolds number is used which is based on the longitudinal velocity in the middle of the channel at the considered distance from the front wall, see also figure 4.3 in the following.

1.3 General equations

1.3.1 Used assumptions

As previously mentioned, flow injection is assumed to be steady and uniform (independent of the location) and strictly perpendicular to the porous wall. Concerning the theoretical results, the geometry is assumed to be constant. In fact, as demonstrated in [8], a slow regression of the porous wall (compatible with the real time scale of the motion of the propellant surface in real motors) does not modify significantly the results presented in the following.

Finally the total length of the channel is assumed to be sufficiently short so that the flow remains subsonic inside the channel (it will be shown below that the flow is uniformly accelerated in the x direction due to the injection). As the temperature field is numerically observed to be more or less constant, we also assume that the flow is incompressible. Again this assumption has been validated, see [9].

1.3.2 Plane geometry

Assuming that the flow remains two-dimensional, all the quantities depend only on the time t and on the spatial coordinates (x, y). The two components of the instantaneous flow velocity are noted $(\tilde{u}, \tilde{v})$, the pressure $\tilde{p}$, so that the Navier-Stokes equations written for the incompressible flow in the cartesian (x, y) coordinate system are :

$$\begin{cases} \dfrac{\partial \tilde{u}}{\partial x} + \dfrac{\partial \tilde{v}}{\partial y} = 0 \\[2ex] \dfrac{\partial \tilde{u}}{\partial t} + \tilde{u}\dfrac{\partial \tilde{u}}{\partial x} + \tilde{v}\dfrac{\partial \tilde{u}}{\partial y} + \dfrac{\partial \tilde{p}}{\partial x} = \dfrac{1}{\mathcal{R}}\Delta\tilde{u} \\[2ex] \dfrac{\partial \tilde{v}}{\partial t} + \tilde{u}\dfrac{\partial \tilde{v}}{\partial x} + \tilde{v}\dfrac{\partial \tilde{v}}{\partial y} + \dfrac{\partial \tilde{p}}{\partial y} = \dfrac{1}{\mathcal{R}}\Delta\tilde{v} \end{cases} \tag{1.1}$$

where Δ denotes the laplacian operator. The boundary equations must first express the no-slip condition together with the injection condition at the two horizontal porous walls. Concerning the front wall, the no-slip condition leads to a non self-coherent relation, especially at the two corners $(0, -1)$ and $(0, 1)$ in terms of (x, y) coordinates. Assuming an injection at these points is not compatible indeed with the viscous no-slip relationship. A possible solution could be to simulate a boundary layer in the injection process in the neighbourhood of these two points. A simpler solution however consists in assuming that the front wall acts as a symmetry plane (allowing a mirror flow for negative values of x). This last solution leads to impose that only the $\tilde{u}$ component vanishes at $x = 0$. Finally the boundary conditions associated to the equations (1.1) are :

$$\begin{cases} \forall y \in [-1, +1] \qquad \tilde{u}(0, y) = 0 \\[1ex] \forall x \geq 0 \qquad \tilde{u}(x, -1) = 0, \quad \tilde{v}(x, -1) = 1, \quad \tilde{u}(x, 1) = 0, \quad \tilde{v}(x, 1) = -1 \end{cases} \tag{1.2}$$

For this type of flow, it may be useful to work with a stream function $\tilde{\psi}$ related to the velocity by :

$$\tilde{u} = \frac{\partial \tilde{\psi}}{\partial y} \qquad \tilde{v} = -\frac{\partial \tilde{\psi}}{\partial x}$$

In system (1.1), the continuity condition is automatically satisfied for $\tilde{\psi}$, whereas the pressure can be eliminated between the two momentum equations. Differentiating the first momentum equation with respect to y and the second one with respect to x and subtracting then these two equations lead to :

$$\frac{\partial}{\partial t}\left(\frac{\partial}{\partial y}\tilde{u} - \frac{\partial}{\partial x}\tilde{v}\right) + \tilde{u}\frac{\partial}{\partial x}\left(\frac{\partial}{\partial y}\tilde{u} - \frac{\partial}{\partial x}\tilde{v}\right) + \tilde{v}\frac{\partial}{\partial y}\left(\frac{\partial}{\partial y}\tilde{u} - \frac{\partial}{\partial x}\tilde{v}\right) = \frac{1}{\mathcal{R}}\Delta\left(\frac{\partial}{\partial y}\tilde{u} - \frac{\partial}{\partial x}\tilde{v}\right)$$

In terms of stream function, this writes :

$$\frac{\partial}{\partial t}\Delta\tilde{\psi} + \frac{\partial \tilde{\psi}}{\partial y}\frac{\partial}{\partial x}\Delta\tilde{\psi} - \frac{\partial \tilde{\psi}}{\partial x}\frac{\partial}{\partial y}\Delta\tilde{\psi} = \frac{1}{\mathcal{R}}\Delta\Delta\tilde{\psi} \tag{1.3}$$

The boundary conditions must then also be expressed in terms of $\tilde{\psi}$:

$$\begin{cases} \forall y \in [-1,+1] \qquad \dfrac{\partial \tilde{\psi}}{\partial y}(0,y) = 0 \\ \forall x \geq 0 \qquad \dfrac{\partial \tilde{\psi}}{\partial y}(x,-1) = 0, \quad \dfrac{\partial \tilde{\psi}}{\partial x}(x,-1) = -1, \quad \dfrac{\partial \tilde{\psi}}{\partial y}(x,1) = 0 \quad \dfrac{\partial \tilde{\psi}}{\partial x}(x,1) = 1 \end{cases} \tag{1.4}$$

1.3.3 Cylindrical geometry

In this case, $\tilde{p}$ remains the notation for the pressure and the three components of the instantaneous velocity write now as $(\tilde{u}_x, \tilde{u}_r, \tilde{u}_\theta)$, in the cylindrical (x, r, θ) coordinate system illustrated in figure 1.5. The Navier-Stokes equations become now :

$$\begin{cases} \dfrac{\partial \tilde{u}_x}{\partial x} + \dfrac{\partial \tilde{u}_r}{\partial r} + \dfrac{\tilde{u}_r}{r} + \dfrac{1}{r}\dfrac{\partial \tilde{u}_\theta}{\partial \theta} = 0 \\ \dfrac{\partial \tilde{u}_x}{\partial t} + \tilde{u}_x \dfrac{\partial \tilde{u}_x}{\partial x} + \tilde{u}_r \dfrac{\partial \tilde{u}_x}{\partial r} + \tilde{u}_\theta \dfrac{1}{r}\dfrac{\partial \tilde{u}_x}{\partial \theta} + \dfrac{\partial \tilde{p}}{\partial x} = \dfrac{1}{\mathcal{R}}\left(\dfrac{\partial^2 \tilde{u}_x}{\partial x^2} + \dfrac{\partial^2 \tilde{u}_x}{\partial r^2} + \dfrac{1}{r}\dfrac{\partial \tilde{u}_x}{\partial r} + \dfrac{1}{r^2}\dfrac{\partial^2 \tilde{u}_x}{\partial \theta^2}\right) \\ \dfrac{\partial \tilde{u}_r}{\partial t} + \tilde{u}_x \dfrac{\partial \tilde{u}_r}{\partial x} + \tilde{u}_r \dfrac{\partial \tilde{u}_r}{\partial r} + \tilde{u}_\theta \dfrac{1}{r}\dfrac{\partial \tilde{u}_r}{\partial \theta} - \dfrac{\tilde{u}_\theta^2}{r} + \dfrac{\partial \tilde{p}}{\partial r} \\ \qquad = \dfrac{1}{\mathcal{R}}\left(\dfrac{\partial^2 \tilde{u}_r}{\partial x^2} + \dfrac{\partial^2 \tilde{u}_r}{\partial r^2} + \dfrac{1}{r}\dfrac{\partial \tilde{u}_r}{\partial r} - \dfrac{\tilde{u}_r}{r^2} + \dfrac{1}{r^2}\dfrac{\partial^2 \tilde{u}_r}{\partial \theta^2} - \dfrac{2}{r^2}\dfrac{\partial \tilde{u}_\theta}{\partial \theta}\right) \\ \dfrac{\partial \tilde{u}_\theta}{\partial t} + \tilde{u}_x \dfrac{\partial \tilde{u}_\theta}{\partial x} + \tilde{u}_r \dfrac{\partial \tilde{u}_\theta}{\partial r} + \dfrac{\tilde{u}_\theta}{r}\dfrac{\partial \tilde{u}_\theta}{\partial \theta} + \dfrac{\tilde{u}_\theta \tilde{u}_r}{r} + \dfrac{1}{r}\dfrac{\partial \tilde{p}}{\partial \theta} \\ \qquad = \dfrac{1}{\mathcal{R}}\left(\dfrac{\partial^2 \tilde{u}_\theta}{\partial x^2} + \dfrac{\partial^2 \tilde{u}_\theta}{\partial r^2} + \dfrac{1}{r}\dfrac{\partial \tilde{u}_\theta}{\partial r} - \dfrac{\tilde{u}_\theta}{r^2} + \dfrac{1}{r^2}\dfrac{\partial^2 \tilde{u}_\theta}{\partial \theta^2} + \dfrac{2}{r^2}\dfrac{\partial \tilde{u}_r}{\partial \theta}\right) \end{cases} \tag{1.5}$$

Concerning the boundary conditions, the same previous remark about the injection at the abscissa $x = 0$, close to the front wall, can be expressed. The boundary conditions are thus :

$$\begin{cases} \forall \theta \in [0, 2\pi[\quad \forall r \in [0,1] \qquad \tilde{u}_x(0, r, \theta) = 0 \\ \forall x \geq 0, \quad \forall \theta \in [0, 2\pi[\qquad \tilde{u}_x(x, 1, \theta) = 0, \quad \tilde{u}_r(x, 1, \theta) = -1, \quad \tilde{u}_\theta(x, 1, \theta) = 0 \end{cases} \tag{1.6}$$

1.4 Basic flow

In this section, we will first determine a particular steady solution of the Navier-Stokes equations and associated boundary conditions. The following step of the analysis will be to determine its stability, this will be done in the following chapters. The physical quantities associated to the steady solution, we are looking for, will be noted in capital and overlined letters.

1.4.1 Plane case

It is possible to find a mathematical steady solution of the equations. A self-similar solution firstly proposed by Berman, see [10], may be sought for the stream function of the mean flow :

$$\bar{\psi} = xF(y)$$

that is $\bar{U} = xF'(y)$ and $\bar{V} = -F$ in terms of the velocity components. Equation (1.3) leads to

$$F'F'' - FF''' = \frac{1}{\mathcal{R}} F^{(IV)} \tag{1.7}$$

associated to the boundary conditions :

$$F(-1) = -1 \qquad F'(-1) = 0 \qquad F(1) = 1 \qquad F'(1) = 0$$

(the boundary condition at the front wall is automatically satisfied with this self-similar form). For large Reynolds numbers, a very accurate approximation of the basic flow is obtained with the so-called Taylor solution, see [11] :

$$\bar{U} = \frac{\pi x}{2} \cos \frac{\pi y}{2} \qquad \bar{V} = -\sin \frac{\pi y}{2} \tag{1.8}$$

which is strictly valid for the equations written for an inviscid flow. The (inviscid) pressure is then given by :

$$\bar{P} = -\frac{\pi^2 x^2}{8} - \frac{1}{2}\left(\sin \frac{\pi y}{2}\right)^2 + P_0$$

where P_0 is a constant. The associated stream function is :

$$\bar{\psi} = x \sin \frac{\pi y}{2} + k$$

with k a constant.

1.4.2 Axisymmetric case

In the cylindrical case, a steady axisymmetric solution may be also determined in the self-similar form given by :

$$\bar{U}_x = \frac{1}{r}\frac{\partial \Phi}{\partial r} \qquad \bar{U}_r = -\frac{1}{r}\frac{\partial \Phi}{\partial x} \qquad \bar{U}_\theta = 0 \qquad \text{with} \quad \Phi(x, r) = x f(r)$$

where Φ is a cylindrical stream function of the flow. The function f satisfies the following differential problem with the prime corresponding to the differentiation with respect to r :

$$\left\{ \begin{array}{l} \dfrac{1}{\mathcal{R}} \left[\dfrac{1}{r} \left\{ r \left(\dfrac{f'}{r} \right)' \right\}' \right]' + \left\{ \dfrac{f}{r} \left(\dfrac{f'}{r} \right)' - \left(\dfrac{f'}{r} \right)^2 \right\}' = 0 \\ \left(\dfrac{f'}{r} \right)' (0) = 0 \qquad \dfrac{f}{r}(0) = 0 \qquad f'(1) = 0 \qquad f(1) = 0 \end{array} \right.$$

The two first boundary equations written above impose the leading order of the behaviour of the function f close to the axis $r = 0$ in case of a viscous flow. Assuming a regular Taylor expansion of the form $f(r) = a_0 + a_1 r + a_2 r^2/2 + \ldots$, it can be readily proved that f satisfies $f(r) = \mathrm{O}(r^3)$ for r close to 0. Without viscosity, only the second boundary condition in $r = 0$ is necessary and the leading order becomes then $f(r) = \mathrm{O}(r^2)$ for r close to 0.

Again it is possible to find an analytical solution, which exactly satisfies the inviscid equations :

$$\bar{U}_x = \pi x \cos \frac{\pi r^2}{2} \qquad \bar{U}_r = -\frac{1}{r} \sin \frac{\pi r^2}{2} \qquad \bar{U}_\theta = 0 \tag{1.9}$$

with the pressure given by :

$$\bar{P} = -\frac{\pi^2 x^2}{2} - \frac{1}{r^2}\left(\sin\frac{\pi r^2}{2}\right)^2 + P_0$$

where P_0 is a constant. This solution constitutes a good approximation of the viscous case for large Reynolds numbers (typically $\mathcal{R} \geq 1000$).

1.4.3 Some remarks

Before analysing the stability properties of the mean flow described above, it may be interesting to note some remarkable features.

- First the approximate analytical solution has been checked to be quasi superposed to the exact self similar solution for the two types of geometry at least for the Reynolds numbers range considered in the present document, see [8] and [12].
- The mean flow depends on two spatial coordinates and accordingly there is a non zero vertical (or radial) velocity component, so that the flow is said to be non parallel. The plane Poiseuille flow, solution in an infinitely long and broad non injected rectangular duct, is strictly parallel, there is only one spatial direction in which the velocity is not homogeneous (the distance to the wall) and consequently the streamlines are strictly parallel. Conversely, the Taylor flow is non parallel, the streamlines start at the porous lines, turn and become more or less parallel far from the front wall. This is illustrated in figure 1.6 for both types of geometry. In fact, even for large values of x, it remains obviously a small region close to the porous wall in which the flow

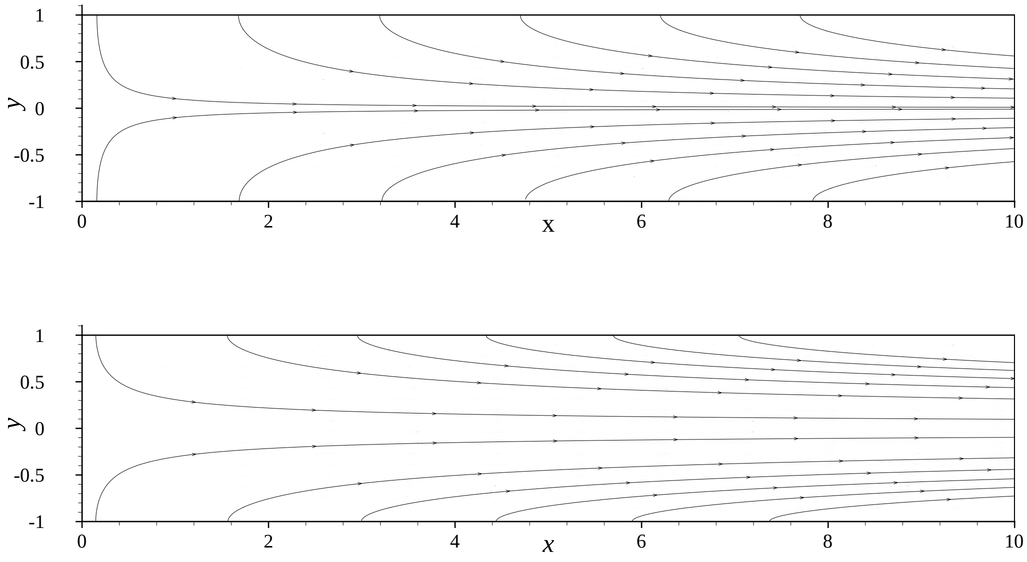

Figure 1.6: (Computed) streamlines of the Taylor flow (plane geometry in the upper figure, axisymmetric geometry in the lower one).

is highly non parallel. This feature induces some difficulties with respect to the mathematical form of the perturbation considered in the stability analysis. This point will be discussed in some details in the following, see section 4.1.

- This x dependence describes explicitly a linear increase of the longitudinal component of the velocity.
- Comparing the two types of geometry in figure 1.6, it appears clearly that at a given x position the curvature of the streamlines is much larger in the axisymmetric case than in the plane case. This will strongly affect the stability results.

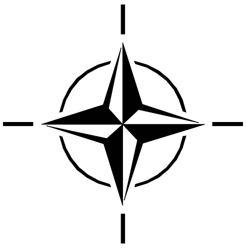

Chapter 2

Linear Stability Theory

2.1 A short philosophical escape

It must be emphasized that the mean flow described in the previous chapter is a possible solution of the equations. However finding such a possible solution does not prove that this solution will be the observed one in practice. This last point depends in fact on the stability of the proposed solution. A similar problem arise for example with a small ball placed on the top of a large sphere (where "top" refers to the direction of the gravity). The position on the top is a possible equilibrium location, however as it is unstable, it cannot be practically observed.

Coming back to the Taylor flow, the same question is relevant : is the particular flow described by expression (1.8) or (1.9) observed in practice, that is for example in the channel VECLA ? In fact the answer depends on the injection conditions (injection velocity and porosity of the material). The injected flow probably contains some turbulent structures which may excite continuously the channel flow. It has been observed that for a given porosity if the injection velocity is too large, the Taylor flow, as it is described by expression (1.8) or (1.9) is never observed. In that conditions, the flow inside the channel is turbulent everywhere, so that it exists large turbulent fluctuations, which interact between themselves leading by nonlinear mechanisms to a modification of the mean flow. The Taylor flow which is a possible solution of the averaged equations does not correspond then to the averaged observed (or measured) flow. This case will be no longer examined in the following part of the present document.

For small injection velocities and for small values of the porosity, the Taylor flow can be observed, at least in the upstream part of the channel. In fact, the measured flow does not correspond exactly to the Taylor flow, it always exists some fluctuations (for example those induced directly from the non-perfect injection system) superimposed to this theoretical solution. As all dynamical systems, the main flow which is continuously excited by the injection system exhibits two types of response with respect to this forcing. First there is the so-called forced response, whose amplitude is of the same order of the forcing amplitude. Secondly it may exist an eigenresponse the amplitude of which can be dangerously larger than the one of the forcing.

The amplitude of the eigenresponse may be in fact extremely large, it means that a micro phenomenon (small inhomogeneity of the injection) can generate a macro feature. This particular behaviour is the signature of an intrinsic instability. Obviously determining the physical characteristics of the eigenresponse is very important (amplification rate, frequency, spatial shape), this is the goal of the stability studies. A well-known and classical presentation of the stability theory is published in [13], whereas a general presentation of the practical use of it in case of the boundary layer which exhibits some common feature with the present basic flow is nicely presented in [14] and finally the first attempt of a theoretical application for the Taylor flow has been done in Russia by Varapaev and Yagodkin and has been translated in [7].

2.2 Small perturbation technique

According to the previous comments, a particular solution (the Taylor flow in the present case) is supposed to be known, its stability is going to be analysed. The instantaneous flow is then assumed to result from a pure superposition of this particular flow, which will be called the "basic flow" in the following, and of a fluctuation to be determined. This is mathematically imposed by writing :

$$\tilde{q} = \bar{Q} + q \tag{2.1}$$

for any physical quantity q (components of the velocity, pressure and also for example temperature, mass flux density in case of compressible fluids). The instantaneous flow is assumed to be realistic, thus it satisfies the general governing equations. The key point for the stability analysis is the following one. As we only focus on an eigenresponse (and not on a forced response), the boundary conditions written for the instantaneous flow must be strictly identical to those imposed for the determination of the basic flow.

Before writing the complete equations, it may be instructive to describe formally the procedure. Let us represent the complete equations together with the boundary conditions by a (non linear) operator $\mathcal{L}$, for example the one corresponding to the Navier-Stokes equations and associated boundary conditions. As explained above both basic flow and instantaneous flow are assumed to satisfy these equations and boundary conditions :

$$\mathcal{L}(\tilde{q}) = 0 \qquad \text{and} \qquad \mathcal{L}(\bar{Q}) = 0 \tag{2.2}$$

According to the superposition (2.1), the first equation becomes : $\mathcal{L}(\bar{Q} + q) = 0$. Then, the operator $\mathcal{L}$ being regularly dependent on the physical quantities, a first order Taylor expansion can be written :

$$\mathcal{L}(\bar{Q} + q) = \mathcal{L}(\bar{Q}) + \mathcal{M}(\bar{Q}).q + NLT$$

where NLT means nonlinear terms with respect to the fluctuating quantities q and $\mathcal{M}(\bar{Q})$ is a linear operator function of the basic flow which applies to the fluctuating quantities. It represents formally the gradient operator of $\mathcal{L}$. In this course, the fluctuation is assumed to be small in comparison to the basic flow : $q \ll \bar{Q}$, so that the nonlinear terms are small in comparison to the linear ones. Indeed in the linear stability theory these nonlinear terms are simply dropped, the previous Taylor expansion is thus simplified into :

$$\mathcal{L}(\bar{Q} + q) \simeq \mathcal{L}(\bar{Q}) + \mathcal{M}(\bar{Q}).q$$

Finally, as both instantaneous flow and basic flow satisfy the equations as expressed by (2.2), previous equation becomes :

$$\mathcal{M}(\bar{Q}).q = 0 \tag{2.3}$$

which represents the linearised Navier-Stokes equations (and boundary conditions). In the general case, the operator $\mathcal{M}(\bar{Q})$ is invertible so that the only solution is $q \equiv 0$, it means that there is no eigenresponse. However is some very specific cases, as for the present Taylor flow, possible non zero eigensolution may be found. This is mainly the case when the basic flow exhibits symmetry properties (usually invariance with respect to spatial and temporal coordinates) inducing then a special mathematical form for the fluctuation. This is described in the next section.

2.3 Normal mode form

In this section, the basic flow is assumed to be dependent on only one spatial variable : y in the plane case and r in the axisymmetric case. This is the parallel assumption. Of course, as mentioned above, this is not strictly the case for the Taylor flow, see section 4.1. In fact, to be more precise, the parallel assumption consists in assuming that only the physical quantities $\bar{Q}$, which are written in the linearised operator (2.3), are dependent on one spatial variable. For example for the plane Poiseuille flow, which is strictly parallel, the pressure depends on x too, but, at least in the incompressible approximation, this pressure term does not appear explicitly in the linearised equations (2.3).

Just to fix the ideas, we will note y the spatial variable in the non homogeneous direction : $\bar{Q} = \bar{Q}(y)$. Then, equation (2.3) represents a system of partial differential equations whose coefficients depend on the basic flow quantities $\bar{Q}$, hence on y only. Thus with respect to each of the other variables, equation (2.3) appears as a system of linear equations with constant coefficients. It is well known that solutions in that case may be sought in an exponential form. Following this mathematical result, all the fluctuating quantities are sought with the so-called normal mode form :

$$\begin{aligned} q(x,y,t) &= \hat{q}(y)e^{i(\alpha x - \omega t)} && \text{plane case} \\ q(x,r,\theta,t) &= \hat{q}(r)e^{i(\alpha x + m\theta - \omega t)} && \text{axisymmetric case} \end{aligned} \tag{2.4}$$

This notation needs to be explained. First, some quantities have complex values, for example i is the imaginary number satisfying $i^2 = -1$, whereas the physical fluctuation must be obviously real. In fact, the physical fluctuating quantities correspond to the real part of the right hand side terms in (2.4). The functions $\hat{q}(y)$ and $\hat{q}(r)$ are complex and are called the amplitude functions, m is an integer and is the azimuthal wave number and α and ω are generally complex numbers. Introducing real part and imaginary part of these two numbers by subscripts "r" and "i", the fluctuating quantities q write :

$$q(x,y,t) = \hat{q}(y)e^{-\alpha_i x + \omega_i t}\ e^{i(\alpha_r x - \omega_r t)}$$

The second exponential term is of norm 1, it describes thus the wavy nature of the solution for the fluctuation, α_r is the longitudinal wave number, ω_r the circular frequency with $f = \omega/2\pi$ being the frequency itself. The first exponential term is real, it describes a possible amplification of the fluctuation with respect to the time and/or with the distance x according to the sign of ω_i and α_i. Usually at this step, two types of theory are distinguished : the temporal theory for which $\alpha_i \equiv 0$, the fluctuations only grow with time and the growth is governed by the temporal growth rate ω_i and the spatial theory for which on the other hand we have $\omega_i \equiv 0$, the fluctuations only grow in x

and the growth is governed by the spatial growth rate $-\alpha_i$. Between these two theories, it may be interesting to recall that in fact both theories usually provide very similar results by using the so-called Gaster transformation, see [15] :

$$-\alpha_i \simeq \frac{\omega_i}{V_g} \qquad \text{with} \quad V_g = \frac{\partial \omega}{\partial \alpha}$$

where V_g is the group velocity (such an approximation is strictly valid in the vicinity of the neutral curve).

As suggested by the experimental results for the Taylor flow, which will be given in section 3.4, the relevant approach in the present case is the spatial theory. The mathematical form of the perturbation used in the present document is thus :

$$q(x,y,t) = \hat{q}(y)e^{-\alpha_i x}\ e^{i(\alpha_r x - \omega_r t)} = \hat{q}(y)e^{i(\alpha x - \omega t)} \tag{2.5}$$

with ω a real number and α a complex one. Assuming that the perturbation is convected in the same direction as the basic flow, that is for increasing values of x, the spatial evolution of the fluctuation and consequently the stability of the basic flow depends on the sign of α_i, the results are given in table 2.1. The same conclusions are true for the perturbation form in the axisymmetric geometry.

sign of α_i	basic flow
$\alpha_i > 0$	stable
$\alpha_i < 0$	unstable
$\alpha_i = 0$	neutral (or marginal)

Table 2.1: Stability criterion in term of spatial amplification growth rate

Finally, the perturbation given by relation (2.4) in the "plane case" corresponds to a plane perturbation. A more general form of the perturbation must include the z-dependence, the perturbation writing then :

$$q(x,y,z,t) = \hat{q}(y)e^{i(\alpha x + \beta z - \omega t)}$$

It is known, see [13] for example, that for a strictly parallel basic flow, it is sufficient to limit the stability analysis to two-dimensional modes, as written in (2.4). This result comes from the so-called Squire's theorem. This one cannot be theoretically applied due to the nonparallel terms which are kept in the stability equations. However, systematic stability computations performed for a three-dimensional perturbation showed that the most amplified mode (which corresponds to the largest growth rate $-\alpha_i$) is obtained for $\beta = 0$, that is for a two-dimensional mode. This explains why the perturbation is assumed to be in the form (2.4) in the following.

2.4 Dispersion relation

The problem now is to determine the amplitude functions, the frequency and of course the complex wave number α. The perturbation is required to satisfy the linearized equations (2.3). Consequently, the form (2.5) is introduced into these linearized equations, this yields :

$$\mathcal{N}(\bar{Q}, \alpha, \omega).\hat{q} = 0$$

where $\mathcal{N}$ is now an ordinary differential operator with respect to y only. Differentiations with respect to t and to x simply become multiplications by $-i\omega$ and by $i\alpha$ respectively. In order to find a non zero solution $\hat{q}$, it is necessary to find values of (α, ω) such as $\mathcal{N}(\bar{Q}, \alpha, \omega)$ is non invertible. The mean flow depends on x and on y but practically the stability analysis is performed for a fixed value of x. On the other hand, as this operator corresponds to the linearized form of the Navier-Stokes equations (1.1), the Reynolds number $\mathcal{R}$ is a parameter. Finally, the formal linearized equations may be written as :

$$\mathcal{N}(x, \mathcal{R}, \alpha, \omega).\hat{q} = 0 \tag{2.6}$$

Now we have to find conditions for which $\mathcal{N}(x, \mathcal{R}, \alpha, \omega)$ is not invertible. Again, it can be first noted that this operator is usually invertible, however it may be possible that for some specific conditions between the parameters $(x, \mathcal{R}, \alpha, \omega)$, the operator is not invertible. These (not known and not obvious) specific conditions are noted by a relation :

$$\mathcal{F}(x, \mathcal{R}, \alpha, \omega) = 0 \tag{2.7}$$

which is called a dispersion relation, because for x and $\mathcal{R}$ being fixed, this equation binds the frequency and the phase velocity ω/α. Of course, this equation is usually not explicit, numerical computations are necessary. They are often performed in two steps (eigenvalues and then eigenfunctions). First, the differential continuous problem being discretised, a complex eigenvalue (α for example) is searched in such a way that a non zero solution for the perturbation may exist. In this step, equation (2.7) is solved in fact, even if the latter is not written explicitly. Then the optional second step consists in determining the non zero solution, with the obtained eigenvalue (which allows a non zero solution). Namely, this non zero solution is the eigenfunction associated to the obtained eigenvalue. Some insight about the numerical aspects are given in appendix.

2.5 Linearised equations

2.5.1 Plane case

As explained before, the small perturbation technique is used, by decomposing each quantity as written in relation (2.1). In this section, the perturbation is written with the normal mode form (2.4) even if it is not justified, according to the x dependence of the mean flow. This problem related to the non parallel effects will be considered in section 4.1.

For the plane case, it is possible to use either the primitive variables (u, v, p) or the stream function. Let us start with the first formulation. The procedure given in section 2.2 leads with (1.1) to :

$$\left\{\begin{array}{l} i\alpha\hat{u} + \dfrac{\partial\hat{v}}{\partial y} = 0 \\ -i\omega\hat{u} + i\alpha\bar{U}\hat{u} + \hat{u}\dfrac{\partial\bar{U}}{\partial x} + \bar{V}\dfrac{\partial\hat{u}}{\partial y} + \hat{v}\dfrac{\partial\bar{U}}{\partial y} + i\alpha\hat{p} = \dfrac{1}{\mathcal{R}}\left(\dfrac{\partial^2\hat{u}}{\partial y^2} - \alpha^2\hat{u}\right) \\ -i\omega\hat{v} + i\alpha\bar{U}\hat{v} + \hat{u}\dfrac{\partial\bar{V}}{\partial x} + \bar{V}\dfrac{\partial\hat{v}}{\partial y} + \hat{v}\dfrac{\partial\bar{V}}{\partial y} + \dfrac{\partial\hat{p}}{\partial y} = \dfrac{1}{\mathcal{R}}\left(\dfrac{\partial^2\hat{v}}{\partial y^2} - \alpha^2\hat{v}\right) \end{array}\right. \tag{2.8}$$

This system is associated to the following boundary conditions, coming from (1.2) :

$$\hat{u}(-1) = \hat{v}(-1) = \hat{u}(1) = \hat{v}(1) = 0$$

It can be easily shown that system (2.8) may be written under the form of a first order ordinary differential linear problem applied to the vector $(\hat{u}, \partial\hat{u}/\partial y, \hat{v}, \hat{p})$ of dimension 4, so that this system, associated to the four boundary conditions above is a well-posed problem. It remains to solve it numerically, see the appendix for some numerical details.

The stream function formulation has the advantage to define only one scalar unknown (the stream function amplitude). The superposition (2.1) is introduced in equation (1.3). After linearisation, this leads to

$$\left(-i\omega + i\alpha\bar{U} + \bar{V}D - \frac{1}{\mathcal{R}}(D^2-\alpha^2)\right)(D^2-\alpha^2)\hat{\psi} - \frac{\partial^2\bar{V}}{\partial y^2}D\hat{\psi} - i\alpha\frac{\partial^2\bar{U}}{\partial y^2}\hat{\psi} = 0 \tag{2.9}$$

where D represents the differentiation with respect to y. This equation corresponds exactly to equation (2.3) in case of equation (1.3). Associated to this equation, the following boundary conditions

$$\hat{\psi}(-1) = D\hat{\psi}(-1) = \hat{\psi}(1) = D\hat{\psi}(1) = 0 \tag{2.10}$$

coming from (1.4), must be satisfied. The stream function of the perturbation is thus required to satisfy again a fourth order homogeneous ordinary differential equation (2.9) associated to four homogeneous boundary conditions. Obviously, the trivial $\hat{\psi} \equiv 0$ remains a possible solution. The goal is to find if for specific conditions between α and ω (dispersion relation), another solution may exist. It is also important to note that equation (2.9) contains three supplementary terms (due to the non zero $\bar{V}$ factor) in comparison with the classical Orr-Sommerfeld equation. The latter is obtained as explained before but for a strictly parallel mean flow, that is with a velocity of the form $(\bar{U}(y), 0)$. These additional terms are those associated with an odd order of derivation in (2.9).

2.5.2 Axisymmetric case

The same procedure can be applied in the axisymmetric geometry. Like the plane case, the basic flow does not depend on r only, so that the normal mode is theoretically not applicable. However using it leads to :

$$\left\{\begin{aligned}
& i\alpha\hat{u}_x + \frac{\partial\hat{u}_r}{\partial r} + \frac{\hat{u}_r}{r} + \frac{im}{r}\hat{u}_\theta = 0 \\
& -i\omega\hat{u}_x + i\alpha\bar{U}_x\hat{u}_x + \frac{\partial\bar{U}_x}{\partial x}\hat{u}_x + \bar{U}_r\frac{\partial\hat{u}_x}{\partial r} + \frac{\partial\bar{U}_x}{\partial r}\hat{u}_r + i\alpha\hat{p} \\
& \qquad = \frac{1}{\mathcal{R}}\left(-\alpha^2\hat{u}_x + \frac{\partial^2\hat{u}_x}{\partial r^2} + \frac{1}{r}\frac{\partial\hat{u}_x}{\partial r} - \frac{m^2}{r^2}\hat{u}_x\right) \\
& -i\omega\hat{u}_r + i\alpha\bar{U}_x\hat{u}_r + \frac{\partial\bar{U}_r}{\partial x}\hat{u}_x + \bar{U}_r\frac{\partial\hat{u}_r}{\partial r} + \frac{\partial\bar{u}_r}{\partial r}\hat{u}_r + \frac{\partial\hat{p}}{\partial r} \\
& \qquad = \frac{1}{\mathcal{R}}\left(-\alpha^2\hat{u}_r + \frac{\partial^2\hat{u}_r}{\partial r^2} + \frac{1}{r}\frac{\partial\hat{u}_r}{\partial r} - \frac{\hat{u}_r}{r^2} - \frac{m^2}{r^2}\hat{u}_r - \frac{2im}{r^2}\hat{u}_\theta\right) \\
& -i\omega\hat{u}_\theta + i\alpha\bar{U}_x\hat{u}_\theta + \bar{U}_r\frac{\partial\hat{u}_\theta}{\partial r} + \frac{\bar{U}_r\hat{u}_\theta}{r} + \frac{im}{r}\hat{p} \\
& \qquad = \frac{1}{\mathcal{R}}\left(-\alpha^2\hat{u}_\theta + \frac{\partial^2\hat{u}_\theta}{\partial r^2} + \frac{1}{r}\frac{\partial\hat{u}_\theta}{\partial r} - \frac{\hat{u}_\theta}{r^2} - \frac{m^2}{r^2}\hat{u}_\theta + \frac{2im}{r^2}\hat{u}_r\right)
\end{aligned}\right. \tag{2.11}$$

This system of linear ordinary differential equations is associated to the boundary conditions :

$$\hat{u}_x(1) = \hat{u}_r(1) = \hat{u}_\theta(1) = 0$$

expressing, as for the plane case, that there is no fluctuating velocity (for determining the eigen-response) at the porous wall. The numerical resolution of system (2.11) presents a (small) difficulty at the axis $r = 0$, as usual when using the cylindrical coordinates system, see [16] for a possible treatment of this singularity.

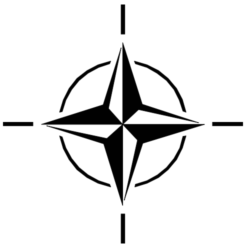

Chapter 3

Stability results

3.1 Eigenmodes

The first task is to determine the solutions of the dispersion relation (2.7) if any. As the conclusions are very similar in the other cases, we will only consider the plane case formulated by the stream function, see (2.9). Then, in order to obtain the "complete" spectrum (i.e. the set of the eigenvalues) of the linearised equations, it is more convenient to fix α and to search all possible solutions in terms of ω for $\mathcal{R}$ and x fixed. The reason comes from the fact that ω appears linearly in the Navier-Stokes equations, and α non linearly because it exists terms in $\partial^2/\partial x^2$ which lead to the factor α^2. More precisely, equation (2.9) may be rewritten in :

$$\left\{\left(i\alpha\bar{U} + \bar{V}D - \frac{1}{\mathcal{R}}(D^2-\alpha^2)\right)(D^2-\alpha^2) - \frac{\partial^2\bar{V}}{\partial y^2}D - i\alpha\frac{\partial^2\bar{U}}{\partial y^2}\right\}\hat{\psi} = i\omega(D^2-\alpha^2)\hat{\psi}$$

which is formally of the type $\mathcal{A}\hat{\psi} = \omega\mathcal{B}\hat{\psi}$, that is of the type of a standard (generalised) eigenvalue problem. The differential problem being discretised, many mathematical libraries allow the determination of the "complete" spectrum.

As an example, the following parameters have been fixed : $\mathcal{R} = 1000$, $x = 10$ and $\alpha = 4$. Some eigenvalues are plotted in figure 3.1 in the complex ω-plane. The horizontal line $\omega_i = 0$ separates the instability zone from the stability zone. The higher the points are, the most dangerous they are (according to the temporal theory). In the instability region, only two amplified modes have been found : $\omega \in \{31.59 + 1.6946i, 31.622 + 1.6296i\}$. They are thus very close together and seem in the figure to be only one. The other modes are damped modes, at least for the chosen values of the parameters. Moreover for smaller value of ω_i it exists many other modes, including possible continuous branches.

To analyse the two amplified modes and their differences, it is generally fruitful to calculate the corresponding eigenfunctions. Moreover, in order to illustrate the strong correspondence between the temporal and the spatial theory, we now move to the spatial theory and fix ω to a real number by $\omega = 31.6$, in the range of the two previous modes. Then by using a shooting method (Newton convergence from an initial guess of the root), two amplified modes are obtained, as in the temporal theory. They are given by $\alpha = 4.0037 - i0.366$ and $\alpha = 4.016 - i0.373$. The group velocity may be calculated, the nearly same value is found for both modes $V_g \simeq 4.4$. Gaster's

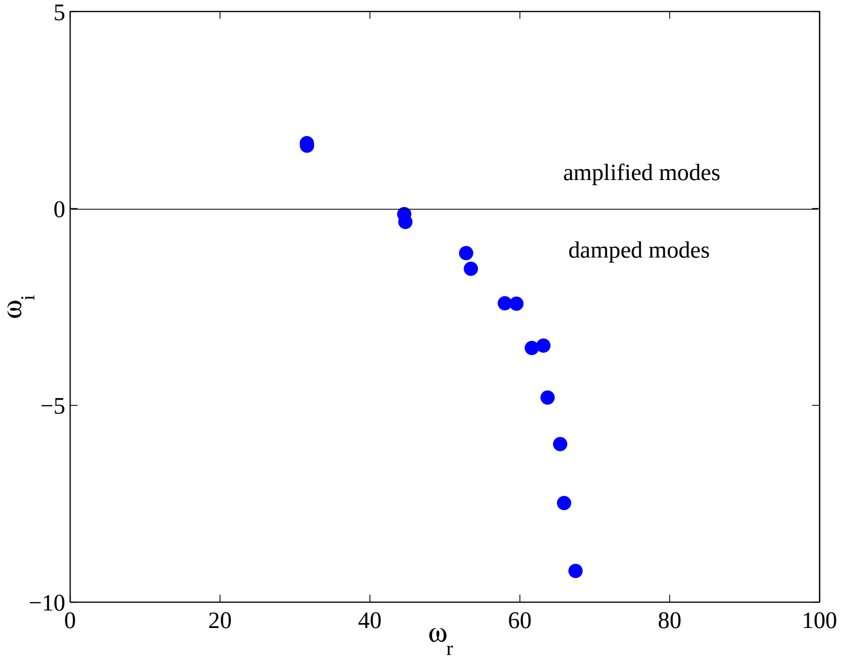

Figure 3.1: Spectrum, $\mathcal{R} = 1000$, $x = 10$, $\alpha = 4$, 300 points in the collocation method

transformation provides then temporal amplification rates which are of order 1.66, they constitute thus good predictions of the temporal growth rates which have been computed directly in the temporal theory.

The corresponding eigenfunctions are plotted in figure 3.2 for the first one and in figure 3.3 for the second one. The main difference between these two modes occurs close to the axis $y = 0$. For the first mode, plotted in figure 3.2, the transverse velocity v is zero on the axis, whereas it is the longitudinal velocity u which vanishes at the axis for the second mode. The first mode is called a varicose mode, and the second one a sinuous mode. Concerning the facility VECLA, it can be noted that with the solid wall (non porous) placed in the upper limit on the duct, only the varicose modes can be observed, the sinuous ones are not compatible with a non-penetration condition at this upper wall.

3.2 Amplitude and n factor

3.2.1 Definition of the n factor

In agreement with the experimental results, see section 3.4 for validations and explanations, the relevant theory is the spatial one, so that ω is a real number characterising the frequency of the wave. The dispersion relation is thus solved for fixed values of $(\mathcal{R}, x, \omega)$ (and additionally with the azimuthal wave number m being fixed for the axisymmetric geometry) and the complex α value is computed in order to satisfy the dispersion relation (2.7).

The opposite of the imaginary part α_i of the complex wave number is the growth rate in

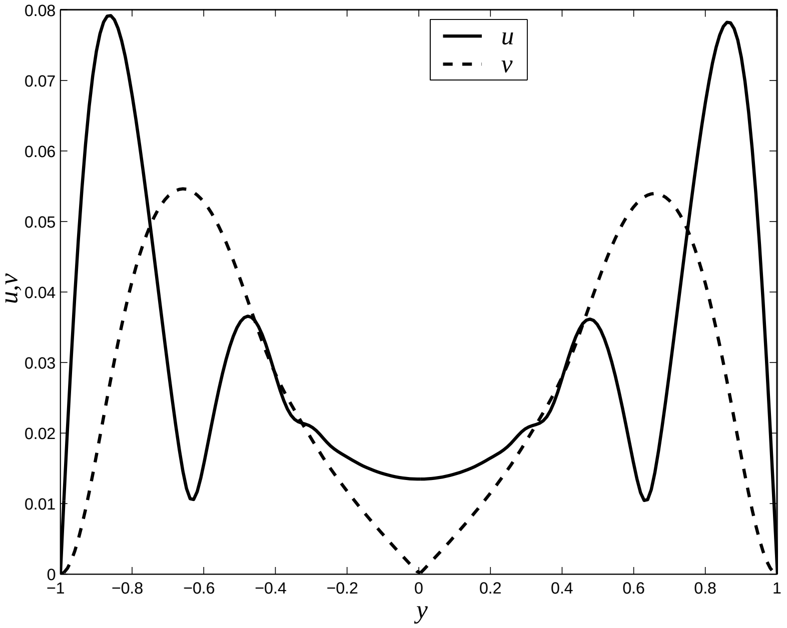

Figure 3.2: Norm of the longitudinal and transverse velocity component of the eigenmode $\alpha = 4.0037 - i0.366$ obtained for $\mathcal{R} = 900$, $x = 10$ and $\omega = 31.6$

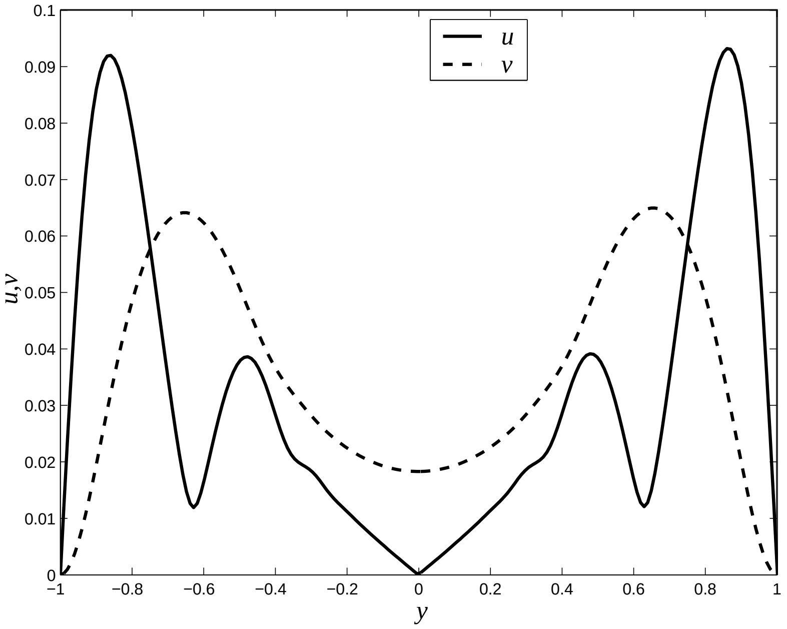

Figure 3.3: Norm of the longitudinal and transverse velocity component of the eigenmode $\alpha = 4.016 - i0.373$ obtained for $\mathcal{R} = 900$, $x = 10$ and $\omega = 31.6$

the x direction. As it has been developed for the boundary layer [17], it is thus possible to define an amplitude A for the eigenmode by :

$$-\alpha_i = \frac{1}{A}\frac{dA}{dx}$$

As suggested by (2.7), the growth rate depends on the parameters $\mathcal{R}$, ω and x. Thus this equation may be integrated in order to calculate the amplitude :

$$A(x;\omega,\mathcal{R}) = A_0 e^n \qquad \text{with} \quad n(x;\omega,\mathcal{R}) = \int_{x_0}^{x} -\alpha_i(\xi;\omega,\mathcal{R})\, d\xi \tag{3.1}$$

With the same meaning as used in the boundary layer, see [18], the factor n gives the logarithm of the eigenmode amplitude. In equation (3.1), x_0 is the neutral position. If it exists, it is the point for given values of $(\mathcal{R},\omega)$ which separates upstream a stable region and downstream an unstable region. Generally, x_0 depends in fact on $(\mathcal{R},\omega)$, so that we may write $x_0 = x_0(\mathcal{R},\omega)$. In equation (3.1) A_0 is an amplitude, which corresponds to the amplitude at the abscissa x_0. It can be noted that the eigenmode is solution of a homogeneous problem, so that its definition is not univocal. For example, with the equation (2.9), if $\hat{\psi}$ satisfies the equation, $\lambda\hat{\psi}$, with λ any complex constant, also satisfies the equation. For that reason, the amplitude A_0 cannot be determined within the linear stability theory. On the other hand, the n factor is intrinsic.

3.2.2 Plane case

To be comparable to the experimental results obtained with VECLA, we only focus on the amplified varicose mode in this paragraph. To give an example, the injection Reynolds number $\mathcal{R}$ is fixed : $\mathcal{R} = 4000$. Then, the growth rate $-\alpha_i$ is computed for different frequencies, and for different values of x. Finally, for each considered frequency, the growth rate is integrated leading to the n factor. The result is given in figure 3.4 in a diagram (x,ω). Some important feature may be deduced from this figure. First there is a critical abscissa, which is close to 5 for the considered Reynolds number[1]. It means that upstream the abscissa $x = 5$, the Taylor flow is stable, possible eigenmodes are damped in this region. On the other hand, downstream the critical abscissa, i.e. for $x \geq 5$, there is a range of frequencies for which the instability modes are amplified. Moreover, it can be noted that this range of "dangerous" frequencies increases with x. However, low frequencies (less than approximately 14) are never amplified, whereas large frequencies become amplified but for more and more large values of x.

The upstream curve corresponds to $n = 0$, i.e. to the neutral (or marginal) curve : the location of $x_0(\mathcal{R},\omega)$ with the notations of (3.1). Without any additional information, it is usually assumed that the amplitude A_0 is a constant at the abscissa $x_0(\mathcal{R},\omega)$. In fact this point is related to the receptivity process which describes the physical mechanism by which eigenmodes appear from the general ambiant turbulent noise or from any other types of excitations. If this ambiant noise does not contain any favoured frequencies, at least in the range of possible amplified frequencies, this uniform repartition of initial amplitude A_0 seems natural as a first approximation. In this case, the n factors give exactly the amplitude of the eigenmodes up to a scale factor. Thus, figure 3.4

---

[1] In fact the exact value of the critical abscissa must be carefully considered. This is due to the non parallel effects which strongly increase for small values of x, see section 4.1.

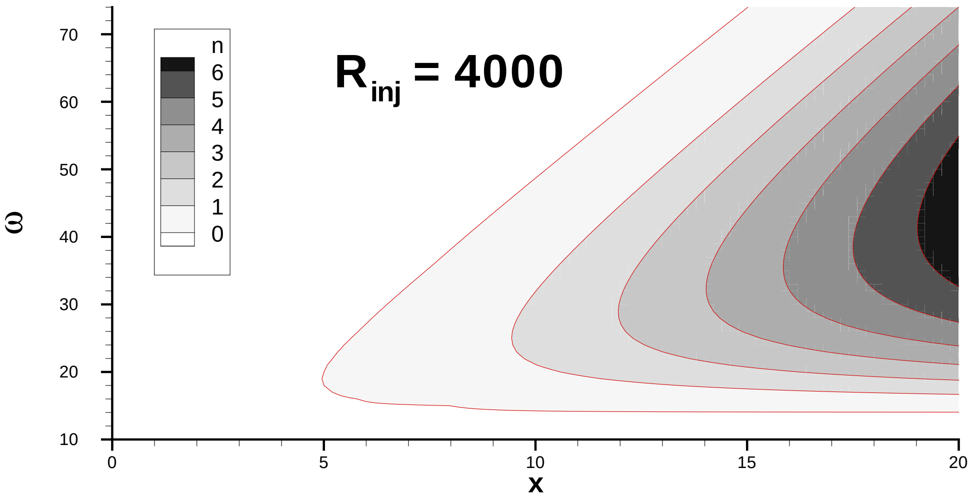

Figure 3.4: Iso-n factors in a (x, ω) diagram, $\mathcal{R} = 4000$

also shows that the frequency which corresponds to the largest eigenmode at a given distance from the front wall is slightly (and quasi linearly) increasing with this distance.

Finally this figure quantifies the amplification, for example, at $x = 20$, the maximum of the n factor is close to 7, it means that the perturbation is $e^7 \simeq 1000$ times larger than the perturbation at $x = 5$.

3.2.3 Axisymmetric case.

For reasonable values of the injection Reynolds number, the frequency and the values of x, only one mode (for each value of the azimuthal wave number) has been found to become amplified from some abscissa. The other modes remain damped. We obviously focus on this possibly amplified mode.

Similarly to figure 3.4, figure 3.5 gives for $m = 0$ (axisymmetric modes) and for the same Reynolds number as before $\mathcal{R} = 4000$, the values of the computed n factor in a diagram (x, ω). The general shape is similar to the one obtained in the plane case. However some important differences exist, that must be noted. First the critical abscissa is located upstream in the axisymmetric case. Furthermore, the n factors seems to be larger in this geometry than in the plane one. For example at $x = 15$, the n factor is close to 11 in the axisymmetric geometry, it is only close to 3 in the plane geometry. Taken into account that the growth of the perturbation follows an exponential behaviour, this means that the axisymmetric Taylor flow is much more unstable than the plane Taylor flow. This difference may be related to the difference observed previously in figure 1.6 between the streamlines in the two cases. Indeed, one important question is to determine the origin of the present intrinsic instability. Even if it is not really demonstrated, it may be suggested that the instability comes from the strong curvature of the streamline close to the porous wall. This could be at least coherent with the following observations.

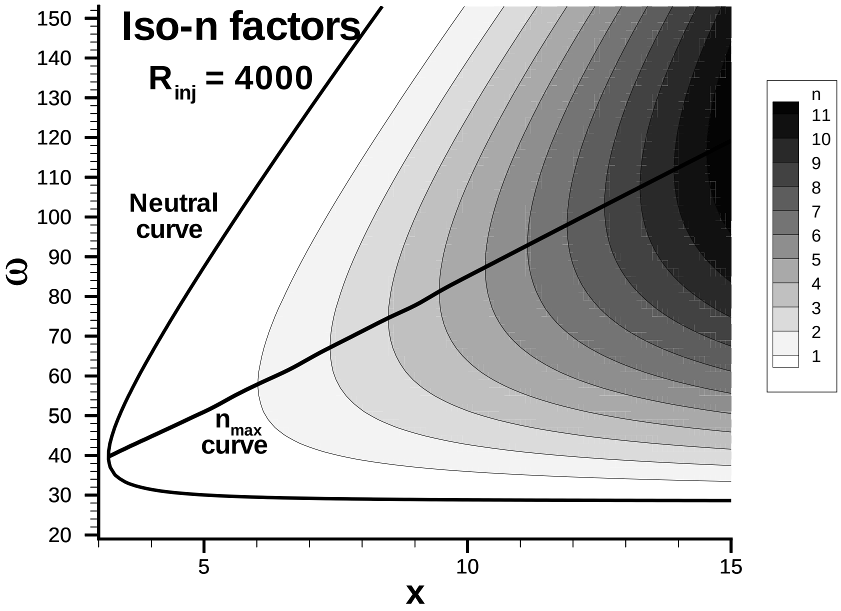

Figure 3.5: Iso-n factor, $m = 0$, $\mathcal{R} = 4000$

1. The maximum of the fluctuating velocity is close to the porous wall.
2. The Taylor flow is stable upstream (where the curvature of the streamlines may be not large enough)
3. If the non parallel terms in $\bar{V}$ are suppressed in the stability equations, such as in (2.8), the basic flow is found to be always stable, see [19].
4. Finally, on one hand, the curvature is much more stronger in the axisymmetric case as in the plane one, as observed in figure 1.6 and, on the other hand, the growth rates are much more larger in the axisymmetric geometry.

The last difference between figures 3.4 and 3.5 concerns the frequency. It seems that the amplified frequencies are greater in the axisymmetric case than in the plane one. For example, the range of amplified frequencies for $x = 8$ is close to $\omega \in [30, 140]$ whereas it is only $\omega \in [15, 40]$ for the plane Taylor flow.

The results given above correspond to the two-dimensional (noted 2D) mode, that is for the azimuthal wave number $m = 0$. An important point concerns the nature of the most amplified mode. A well-known result is the Squire's theorem, which expresses that for a 2D strictly parallel basic flow, the first instability occurs for a 2D perturbation. However, it does not mean that a two-dimensional perturbation is always more amplified than any three-dimensional perturbation, see [20] for more information. However for the Taylor flow this theorem cannot be applied even in the plane case, considering that the stability equations contain some nonparallel terms which makes unapplicable the mentioned theorem. Some direct computations in the plane case show however that the most amplified modes are approximately two-dimensional, these are the varicose and the sinuous modes. For the axisymmetric geometry, figure 3.6 shows the neutral curve and the location of the maximum of the n factor in the (x, ω) diagram for the four first positive azimuthal wave numbers. The first observation is that the results for $m = 0$ and $m = 1$ are quasi identical. This conclusion exactly corresponds to the similarity between the varicose and the sinuous modes previously observed for the plane geometry. On the other hand, larger azimuthal wave numbers seem to be less and less amplified, except for the high frequencies, for which the differences seem to be small. However the critical abscissa for $m = 3$ is close to the one of $m = 0$, for example it is clearly upstream the location of the $n = 1$ curve in figure 3.5. This means that if all the eigenmodes (characterised by (m, ω)) start with the same initial amplitude A_0 at their neutral curve, the amplitude of the $m = 0$ mode at the critical abscissa of $m = 3$ is only a little larger than the amplitude of the $m = 1, 2, 3$ modes. Therefore, it is clear that at a given x position, $x = 7$ for example, the perturbation should be the superposition of several modes corresponding to different values of m, so that for any hot wire measurement it should be very difficult to isolate the contributions of the different modes.

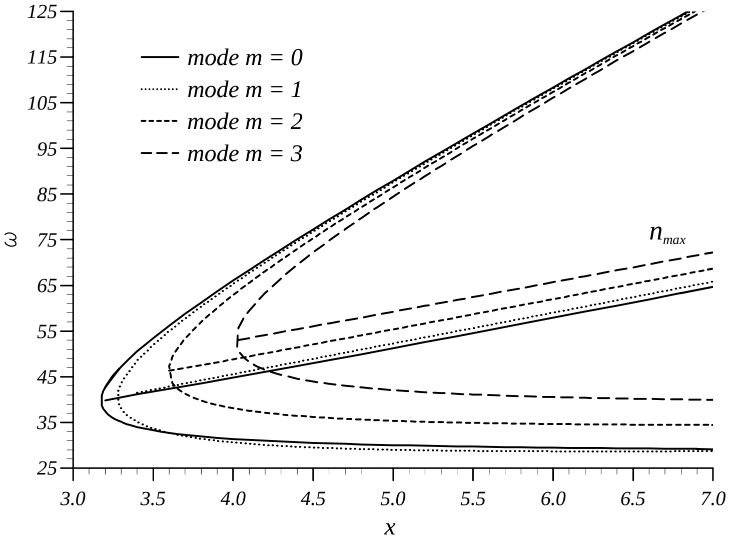

Figure 3.6: Marginal curves for $m = 0, 1, 2, 3$, $\mathcal{R} = 4000$

To conclude this overview of the typical stability results, it remains to analyse the real part of the complex wave number α. It is then more suitable to work with the wavelength λ which is defined by : $\lambda = 2\pi/\alpha_r$. Figure 3.7 gives the iso-λ values, always in a (x, ω) diagram for the axisymmetric geometry with $\mathcal{R} = 4000$ and $m = 0$. It is interesting to note that at least for values of x less than 15, the wavelength of the mode which corresponds to the largest amplitude is close to 1. With a dimensional point of view, this means that the largest mode presents a wavelength roughly equal to the radius of the duct. In particular the streamwise evolution of the

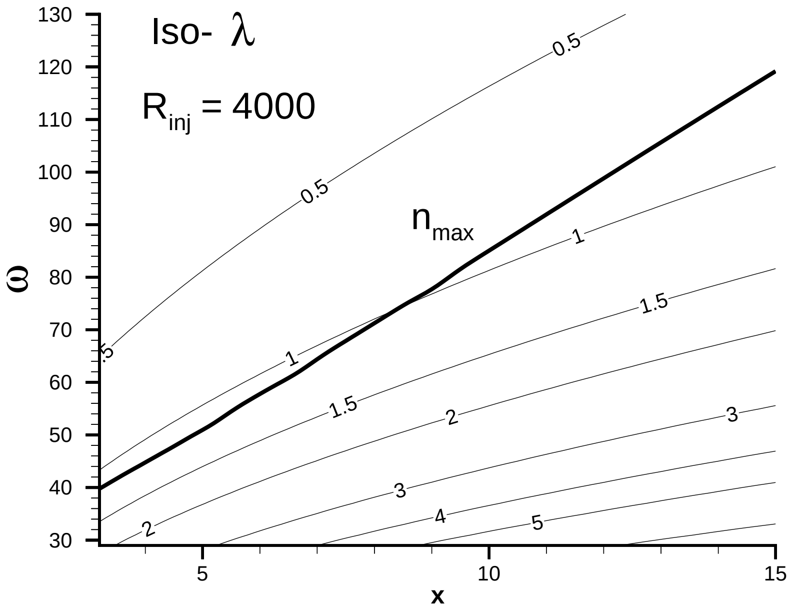

Figure 3.7: Iso-wavelength for $m = 0$, $\mathcal{R} = 4000$

eigenmodes occurs on a scale which is much shorter than the total length of the duct which scales the undesirable cavity modes. Due to this great difference of streamwise extend, it may be guessed that the instability alone is not very efficient as a possible exciting source of the cavity modes.

3.3 Influence of the Reynolds number

Concerning the dispersion relation, the influence of the different parameters x, ω and the azimuthal wave number for the axisymmetric geometry have been studied. It remains the influence of the injection Reynolds number. For example, the plane geometry is considered, with fixed x and ω values : $x = 10$, $\omega = 31.6$ (which have been chosen in the spectrum analysis of the linearised operator, see figure 3.1). The result is plotted in figure 3.8 for the streamwise wave number α_r represented in dashed line and for the growth rate $-\alpha_i$ represented in full line. In this figure, the basic flow is always the one given by the analytical Taylor form (1.8) and only for the stability the Reynolds has been varied from 50 up to 10^5. It is clear that there is an asymptotic behaviour when the Reynolds number increases. This means that the basic mechanism of this instability is mainly inviscid. Up to now, a clear physical explanation “with the hands” of the origin of the instability has not be found. As explained in the previous section, the instability appears to be related to the strong curvature of the streamlines of the mean flow close to the injecting wall, which is little affected by the viscosity.

However the wave number seems to tend to the inviscid value faster than the growth rate. Thus, especially for the estimation of the n factor in practical case for which the Reynolds number

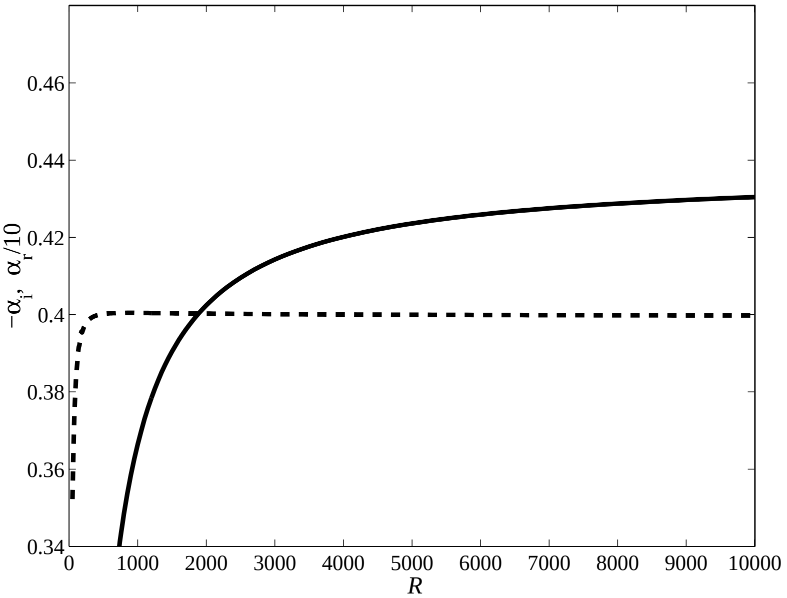

Figure 3.8: Influence of the Reynolds number on the complex streamwise wave number α, plane case, $x = 10$, $\omega = 31.6$, varicose mode. The growth rate $-\alpha_i$ is in full line, the tenth of the wave number $\alpha_r/10$ in dashed line

is of order 1000, it is necessary to take into account the viscous effects, the difference could be of about 10% for inviscid computations. On the other hand, it is important to emphasize that for the mean flow, it is really not necessary to use the viscous mean flow given by (1.7) for Reynolds numbers greater than 100, the Taylor solution is accurate enough.

The same feature can be observed in the axisymmetric geometry, leading to the same conclusions.

3.4 Comparisons with the experiment

3.4.1 Preparation of the results for the comparison

Hot wire measurements give access to the instantaneous velocity at the position where the probe has been placed. Then, using different possible treatments of the signal, the latter is decomposed in two parts : the mean value and the fluctuating one upon which a Fourier transform is applied in order to get the spectral dependence of the fluctuating velocity or more often the power spectral density (DSP).

This spectral representation may be compared to the theoretical predictions. For each given frequency, the n factor is computed by integrating in x the amplification growth rate, so that the amplitude of the fluctuation is simply theoretically given by $A_0 \exp(n(x, \omega))$, with A_0 the initial amplitude coming from the receptivity conditions. In the following results, this constant A_0 is assumed to be independent of ω, but to be a function of the experimental conditions (values of the injection velocity, of the height of the duct, of the porosity of the injecting walls, ...). Obviously, A_0

is independent of x. Consequently for given experimental conditions, the constant A_0 is adjusted once, in order to fit for one frequency and one value of x the measured amplitude. In case of comparisons including y variations, the same constant A_0 must be considered of course.

3.4.2 Effects of the dimensional height of the duct and injection velocity

It is interesting to test first the scaling effects by varying experimentally the injection velocity and the height. From the theoretical point of view, as the computation of the n factor in the (x, ω) plane is performed with dimensionless quantities, changing the injection velocity and the height only modifies the Reynolds number. Comparisons with measurements obtained with the VECLA facility are reported in figure 3.9. Four comparisons are given, they correspond to four values of the pair (injection velocity V_{inj}, height h). The measured values are plotted in full line, the theoretical predictions by the open circles. In the four cases, the frequency is plotted between 0 and 2000 Hz. However the scale of the vertical axis, giving the amplitude of the fluctuation, differs from each other. The adjusted initial amplitude A_0 is also given for each comparison in the legend, it seems that the constant A_0 increases with the injection velocity and decreases with the height of the duct.

The overall comparison is quite satisfying (good prediction of the amplified frequencies and quite good shape of the spectral dependence), even if there are some differences which are mainly visible for $h = 10$ mm. It may be remarked however that for this height (the smallest one for the VECLA facility), the mean flow does not exactly coincide with the theoretical Taylor flow (or the viscous solution), it seems that small three-dimensional structures slightly modify the streamwise component of the mean velocity in comparison with the expected one. However the broadness of the amplified frequencies peak as well as the frequency associated to this peak are in good accordance with the linear stability results.

A similar comparison has been done for the axisymmetric geometry with the available experimental results, see [5]. However in this case, the experiment have been carried out in 1990, that is before the knowledge of the intrinsic instability described in the present document. Among other comparisons, which can be found in [16], figure 3.10 shows the power spectral density of the fluctuating axial velocity for three values of the injection velocity. The latter is represented by M_w, the wall injection Mach number. The left figures (experiment) are directly scanned from the publication, whereas the right ones give the theoretical results obtained for the four first positive azimuthal wave numbers. Three different initial amplitudes A_0 have been chosen for the three different injection velocities. As before, the range of the amplified frequencies seem to agree quite well with the experimental results, even if there are some discrepancies which are significantly larger than the ones observed with VECLA in the plane geometry.

3.4.3 Streamwise amplification

The previous comparisons proved the good agreement between the experimental results and the theoretical ones in terms of range of amplified frequencies. The goal of this section is to analyse carefully the instability process itself, that is the streamwise amplification, which is theoretically of exponential type. The fluctuating velocity at different values of x must be then compared in the same experimental condition (in order to keep the same initial amplitude A_0 for the different

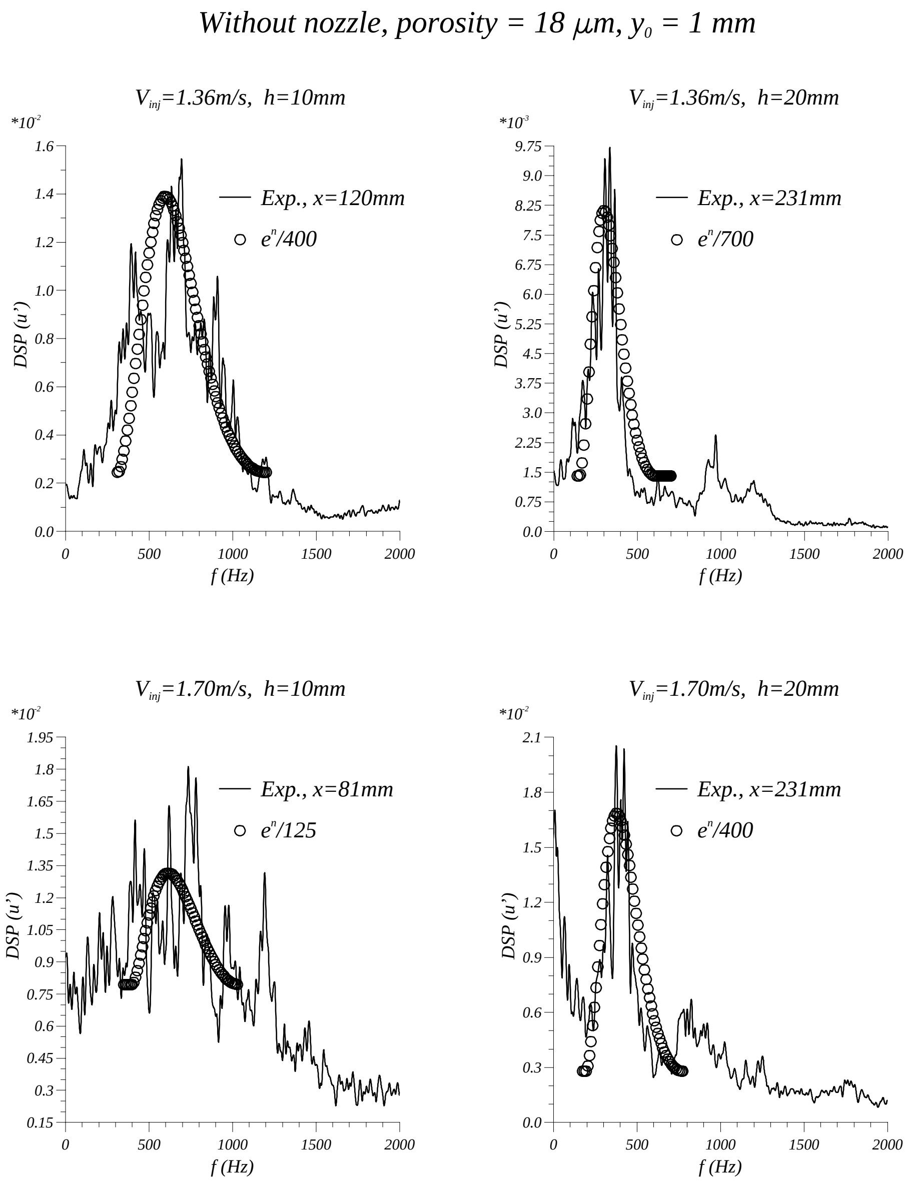

Figure 3.9: Comparisons between LST results and experimental ones with the VECLA facility

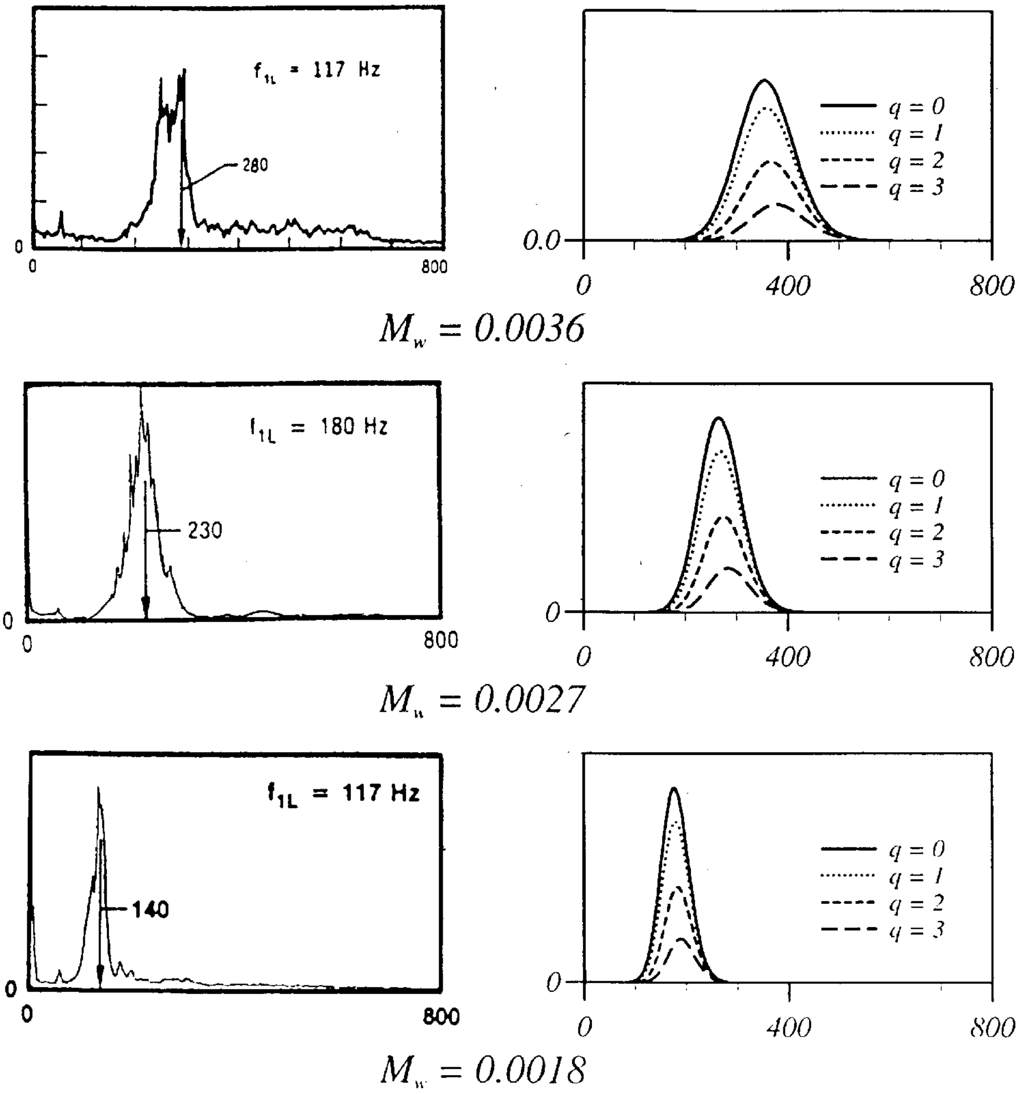

Figure 3.10: Comparisons between LST results and experimental ones obtained by Brown and co-workers

values of x).

A first comparison is given in figure 3.11. The height of the duct is 30 mm. The experimental results (lines) are given in six increasing abscissa, whereas the theoretical values (symbols) are reported for only the four largest values of x. The two first values are indeed upstream the critical abscissa. The comparison gives an excellent agreement between the experiment and the theory demonstrating undoubtedly on one hand the real existence of intrinsic instability for this type of flow and on the other hand the reliability of the present linear stability theory. To emphasize this comparison, let us mention : the range of amplified frequencies (as shown above), the streamwise amplification (as previously said, the same constant $A_0 = 1/6000$ has been used for the different abscissa). Furthermore, the increasing shift of the amplified frequencies with respect to x is also clearly visible in this figure. Finally, the spectrum measured at $x = 570$ mm, the most downstream

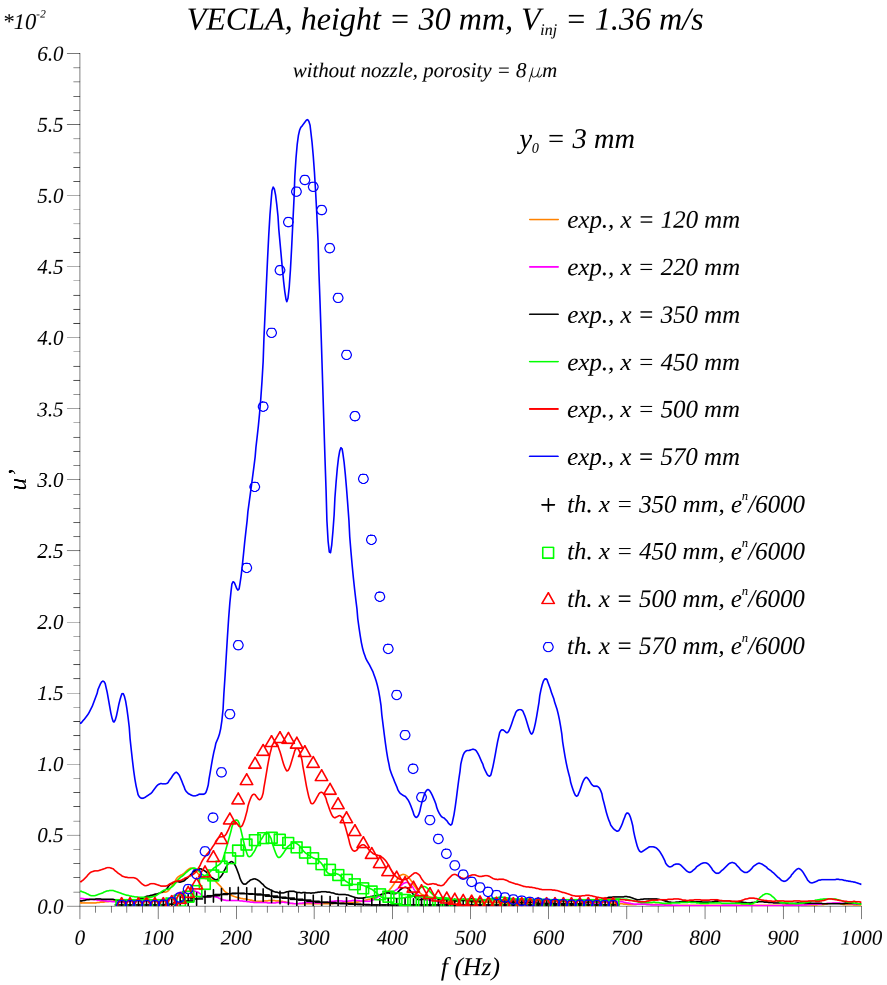

Figure 3.11: Comparisons between LST results and experimental ones with the VECLA facility

position, exhibits an interesting (weakly) nonlinear phenomenon, that is the increase of 2ω and 0ω (steady) modes. These first nonlinear mechanisms are quite well understood in the framework of the boundary layer stability, see [21]. The basic reason comes from the linear form

$$u_\varphi = \frac{1}{2}(\hat{u}\exp(i\omega) + \hat{u}^*\exp(-i\omega))$$

of the physical fluctuation (where z^* represents the complex conjugate of z). The quadratic terms in the Navier-Stokes equations are formally expressed by the product $u_\varphi u_\varphi$. The product is converted into a sum of the exponential terms, leading thus to the frequencies 2ω and 0. And, as the linear step does not amplify only one mode, but a rather broad range, the quadratic interactions lead also to amplify a certain range around zero and another one corresponding to twice the linear range.

Similar comparisons can be also tested with the axiymmetric duct. In the present document,

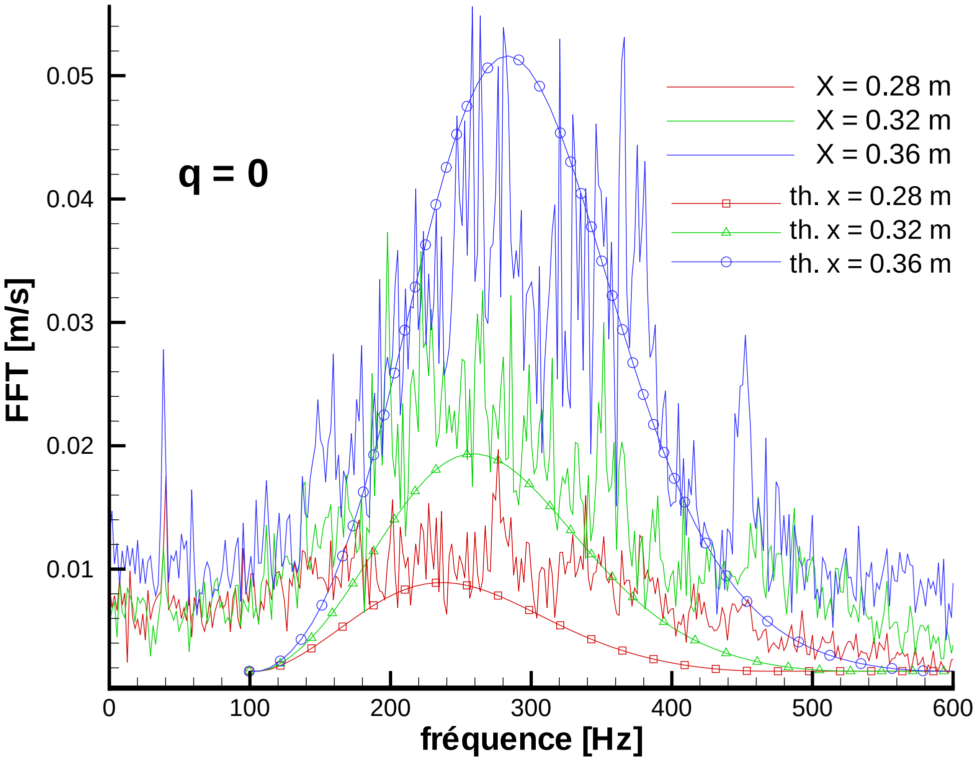

Figure 3.12: Comparisons between LST results and experimental ones obtained with the facility of the VKI. The full lines correspond to the experimental results, each of them at one value of x. They are ordered regularly : the large the FFT amplitude, the larger the value of x.

two different comparisons are shown, the experimental results coming from two different facilities. The first one is located in VKI and the results have been obtained by J. Anthoine, see [6]. As before, the axial fluctuating velocity spectrum is compared between both approaches, the results are given in figure 3.12. The injection velocity is 0.88 m/s, the radius of the duct 38 mm. The spectra are given for three values of x, between 7.4 and 10 in terms of dimensionless distances from the front wall. In comparison with the result given for the plane geometry, it appears immediately that the measured velocity is much less smooth than in figure 3.11.

Similar behaviour have been recently obtained by using the facility VALDO, see [22]. The results are reported in figure 3.13. The radius is 30 mm, the injection velocity 1.05 m/s, the chosen abscissa are thus close to 10.5 in dimensionless value.

From both figures, it may be concluded that there is a range of amplified frequencies which correspond roughly to the theoretical predictions. It seems also that there is a streamwise amplification but some discrepancies are clearly present between the theoretical results and the experimental ones. It is not easy to explain the reason of this noisy signal obtained in the axisymmetric facility. This may be due to the existence of several modes (associated to different azimuthal wave numbers), but this may be also due to the measurement anemometer. In the plane case, the hot wire is parallel to the porous wall whereas in the other geometry, some corners effects may occur. As the probe is placed very close to the porous boundary, there are possible interactions between the mean flow and the corners of the probe which carry the hot wire itself. Anyway, it may be noted that the streamwise amplification is very large. For example, the result shown in figure 3.13 exhibits a huge amplification (factor about 20 in the experiment over a distance of only 1.5 cm).

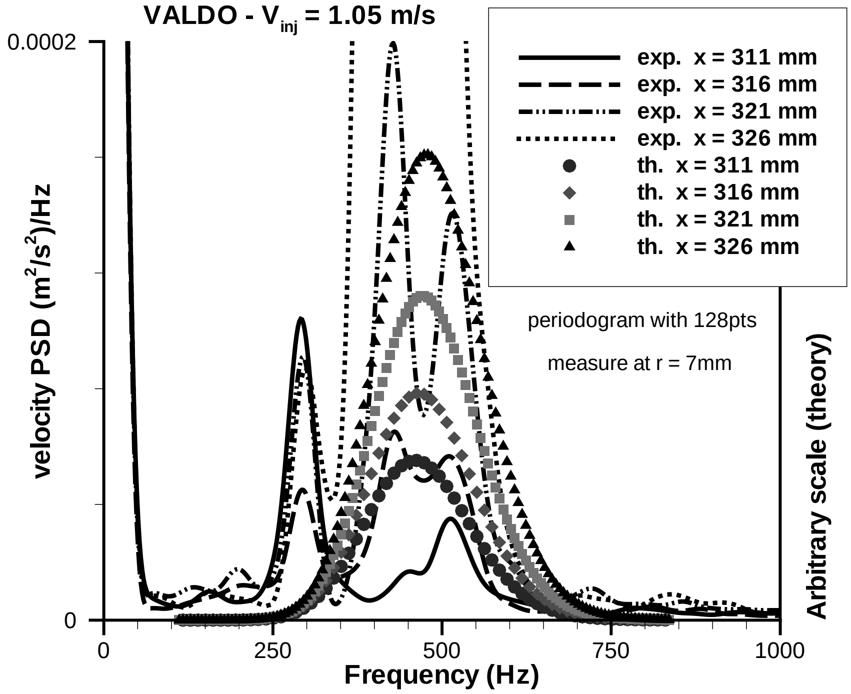

Figure 3.13: Comparisons between LST results and experimental ones obtained with the VALDO facility. Each curve corresponds to one of the four measurements, the same is true for the symbols giving the theoretical predictions

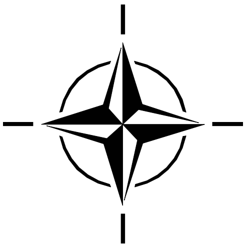

Chapter 4

In(tro)spection of the used assumptions

Different assumptions have been made, their influences must be inspected in order to determine the generality of the results presented in the previous chapter.

4.1 Non parallel effects

4.1.1 Definitions

As explained before, the basic flow explicitly depends on the streamwise coordinate x so that the exponential form $\exp(i\alpha x)$ used for the perturbation is not theoretically justified. For a two-dimensional basic flow, a dependence of the streamwise velocity coordinate with respect to x is related to a non zero transverse velocity $\bar{V}$ through the continuity equation. This is the reason why this x dependence is called a non parallel effect. In the following, the basic flow is assumed to be dependent on x (even weakly).

For clarity, let us call the parallel approach the one when only the $\bar{U}$ is kept in the stability equations (leading to exactly the Orr-Sommerfeld equation) and the nonparallel approach the one for which all terms related to the basic flow are kept in the stability equations. Then, if the perturbation has the form of a normal mode for a parallel basic flow (or for a flow of which the non parallel terms are neglected), the corresponding approach will be noted by OSE (for Orr-Sommerfeld Equation). On the other hand, the (theoretically not justified) use of the normal mode for a non parallel basic flow will be noted by NNP (for Normal Non Parallel approach). All the results shown in the previous chapter have been obtained by using the NNP approach.

Now there are some questions : is the Taylor flow weakly non parallel (so that OSE is a more or less accurate approximation) ? Is it possible to justify the use of NNP ? Is it possible to perform a consistent and accurate non parallel stability analysis ? The following part of the present chapter is aimed to provide some answers to that questions.

4.1.2 Use of a parallel approximation ?

As explained above, the non parallel effects are connected with the magnitude of $\bar{V}$ with respect to $\bar{U}$. Using the Taylor analytical form (1.8), the ratio $\bar{V}/\bar{U}$ may be readily calculated :

$$\left|\frac{\bar{V}}{\bar{U}}\right| = \frac{2}{\pi x}\frac{\left|\sin\frac{\pi y}{2}\right|}{\cos\frac{\pi y}{2}} = \frac{2}{\pi x}\tan\frac{\pi|y|}{2}$$

This suggests that this ratio varies from 0 (at the symmetry axis) to ∞ at the porous walls. However if the dependence on y is suppressed by a norm such as the maximum with respect to y, the ratio is simplified into $\bar{V}/\bar{U} = 2/\pi x$, which indicates that, according to this choice of norm, the non parallel effects decrease with respect to x (the ratio is smaller than 0.05 for $x \geq 15$ for example). From these simple two remarks, it can be concluded that the Taylor flow may appear more and more parallel for large values of x but, reciprocally, at any values of x it exists a small region close to the injecting walls where the basic flow is strongly non parallel.

In order to illustrate the non parallel effects, a first possibility consists in solving the OSE with the streamwise velocity component $\bar{U}$ being the one given by Taylor, even if the mean flow given by the velocity $(\pi x/2\cos(\pi y/2), 0)$ obviously does not satisfy the steady equations. Figure 4.1 gives for the axisymmetric Taylor flow, with $\mathcal{R} = 4500$, $q = 0$ and $\omega = 80$, the evolution with respect to x of the complex number α solved by the OSE, the NNP and the PSE approaches (see below for some explanations on the PSE method). It appears that on one hand NNP and PSE results are very similar, whereas OSE strongly differs from the two others, for example the growth rate remains always positive. Similar behaviour has been found in plane geometry, see [19].

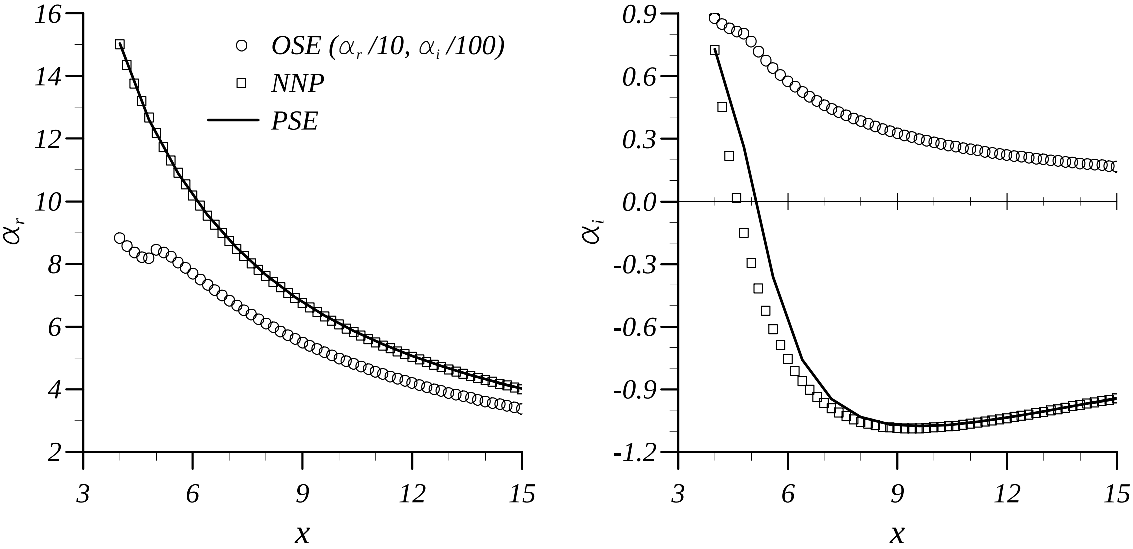

Figure 4.1: Comparison of OSE, NNP and PSE results for the axisymmetric Taylor flow, $\mathcal{R} = 4500$, $q = 0$ and $\omega = 80$. The wavenumber α_r is plotted in the left hand side, the growth rate α_i in the right hand side

This strong non parallel effect is also confirmed by the whole spectrum obtained with the OSE linearised operator with the same values of the parameters are for figure 3.1. The results are given in figure 4.2. Once more, the real part is completely different and no amplified mode has been found. Let us recall that the experiment clearly shows amplified modes which are in relative good agreement with the NNP results. The parallel OSE approach does not seem to be an approximation of the stability results for the present basic flow.

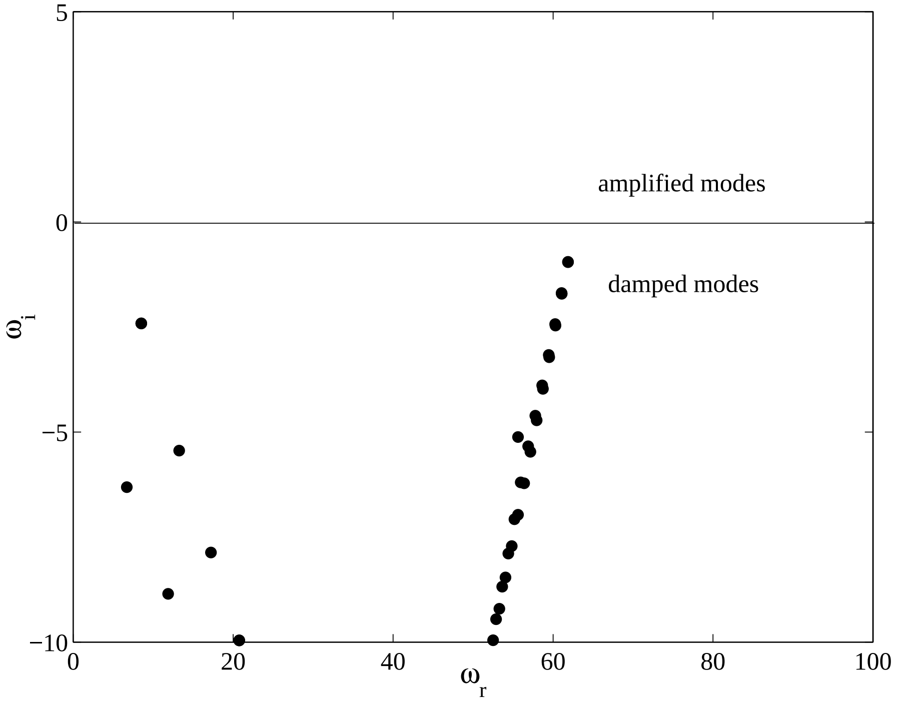

Figure 4.2: Spectrum of the artificially parallel Taylor flow, $\mathcal{R} = 1000$, $x = 10$, $\alpha = 4$

4.1.3 What is the matter with the normal non parallel approach ?

As firstly remarked by comparing results between those of Varapaev and Yagodkin [7], those of Lee and Beddini [23] and ours [19], there is a problem somewhere. Finally the explanation has been found by Griffond [24], the NNP approach is not consistent, because the stability problem depends on the formulation which is used. In the present course, two formulations have been used in the plane case : with the primitive variables (u, v, p) see system (2.8) and with the stream function ψ, see equation (2.9). The matter is to determine if both formulations are strictly equivalent. Before introducing the normal mode, both formulations (1.1) and (1.3) are obviously equivalent as well as the linearised equations deduced from each of them. But, as the normal mode is not and cannot be justified, the question of the equivalence between system (2.8) and equation (2.9) remains posed.

The answer given in [24] is the following one. From system (2.8), the amplitude function of the pressure $\hat{p}$ may be eliminated by multiplying the third equation of that system by $i\alpha$, differentiating the second one (with respect to y) and finally by subtracting both obtained equations. Then in this new equation, the amplitude functions $\hat{u}$ and $\hat{v}$ may be replaced by respectively $-i\alpha\hat{\psi}$ and $D\hat{\psi}$ where $\hat{\psi}$ is an amplitude function for the stream function and D the differentiation operator with respect to y. If we proceed in this way, the following equation is obtained

$$\left(-i\omega + i\alpha\bar{U} + \bar{V}D - \frac{1}{\mathcal{R}}(D^2-\alpha^2)\right)(D^2-\alpha^2)\hat{\psi} - \frac{\partial^2\bar{V}}{\partial y^2}D\hat{\psi} - i\alpha\frac{\partial^2\bar{U}}{\partial y^2}\hat{\psi} + \frac{\partial U}{\partial x}\alpha^2\hat{\psi} = 0 \qquad (4.1)$$

which is NOT equation (2.9) as it ought to be in a consistent theory, the last term of (4.1) is not present in (2.9). Let us just recall that for a strictly parallel basic flow, both formulations are strictly equivalent, they lead both to the Orr-Sommerfeld equation.

The NNP approach is consequently not consistent, its results may depend on the formulation. To illustrate that point, comparisons between the two formulations have been performed, they are illustrated in figure 4.3. In addition, the published results of [7] and [23] have been indicated in symbols. The neutral curve has been calculated for $\mathcal{R} = 100$ for both sinuous and varicose modes and with the two formulations. It is represented in the $(R_c^{1/3}, \alpha_r)$ diagram, where R_c represents the Reynolds number based on the axial velocity (which is linearly dependent on x). All the published results seem to be accurately calculated, the differences between the full lines and the dashed or the dotted ones are intrinsic, they are due to the choice of the normal mode which is inconsistent with the present basic flow.

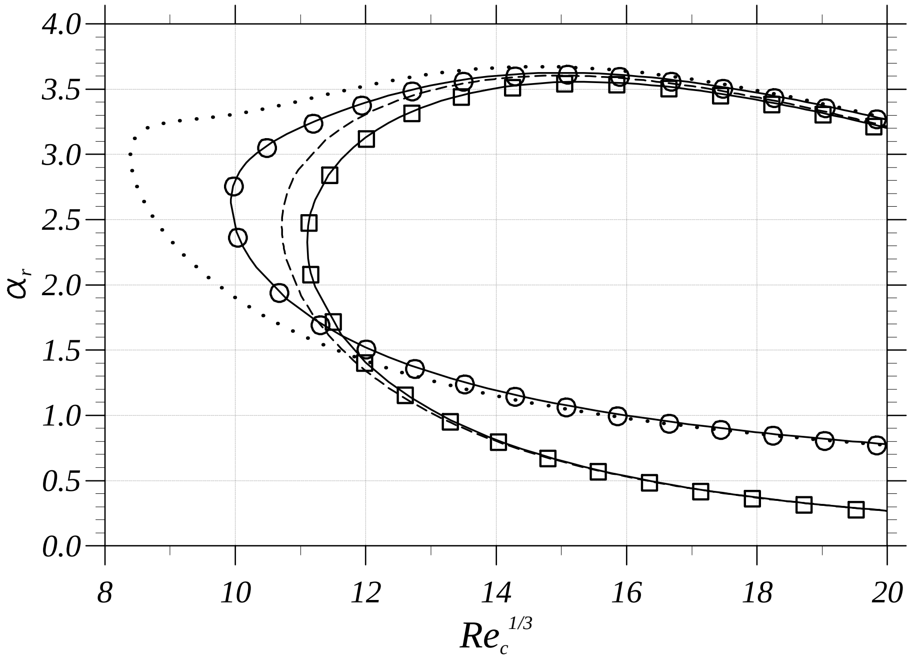

Figure 4.3: Comparisons between diverse published results and our results illustrating the inconsistency of the normal non parallel approach. Using the stream function formulation, results for the neutral curve for the sinuous modes in [7, 23] (circles) and for the varicose modes in [23] coincide with ours (full lines). They are significantly different from ours obtained with the primitive variable formulation for the varicose mode (dashed line) and for the sinuous mode (dotted line). Self-similar solution is used for the plane basic flow with $\mathcal{R} = 100$.

4.1.4 Is there any consistent and accurate non parallel approach ?

From a practical point of view, the inconsistent approach seems however to work with enough accuracy. For large Reynolds number as well as for large values of x, the differences between the two approaches discussed in the previous paragraph are quasi negligible. Furthermore, as shown in the previous chapter, the agreement with the experimental results is very good. Even for the axisymmetric geometry, for which the growth rates are larger and the involving x values smaller, it may be guessed that for practical prediction the NNP approach provides a satisfactory estimation of the instability.

On the other hand, the present solution is clearly wrong for the small values of x. In particular the location of the neutral curve must be considered with care. Thus an alternative approach for the mathematical form of the perturbation, which would be more consistent and more accurate with respect to the non parallel characteristics of the basic flow, would be useful.

Some approaches already exist which are first consistent and whose goal secondly is to deal with the non parallel effects. The clearest one is based on the multiple scale analysis, see [25] or [26] for a general presentation and see [27] for an example of use in a non parallel stability analysis (in the framework of the boundary layer stability). A more recent approach, called PSE (for Parabolized Stability Equations), developed by Herbert and Bertolotti [28], also deals with the non parallel effects. This approach has been used for the present mean flow, the results are shown in figure 4.1. They prove that after a numerical transient in x, the PSE results rapidly agree with the NNP ones. Concerning the consistency, the multiple scale analysis is fully consistent, the PSE approach is quasi consistent, see [29] for more details. The (theoretical) problem with these approaches is that both consider the Orr-Sommerfeld equation as a first order solution, whereas it is not the case for the Taylor basic flow.

Another mathematical form for the perturbation has been proposed by J. Griffond, see [24]. The starting equation is the linearised form of the Navier-Stokes equations expressed with the stream function (1.3). Using the perturbation technique $\tilde{\psi} = \bar{\psi} + \psi$, the linearised problem is :

$$\frac{\partial}{\partial t}\Delta\psi + \frac{\partial\bar{\psi}}{\partial y}\frac{\partial}{\partial x}\Delta\psi + \frac{\partial}{\partial x}\Delta\bar{\psi}\frac{\partial\psi}{\partial y} - \frac{\partial\bar{\psi}}{\partial x}\frac{\partial}{\partial y}\Delta\psi - \frac{\partial}{\partial y}\Delta\bar{\psi}\frac{\partial\psi}{\partial x} = \frac{1}{\mathcal{R}}\Delta\Delta\psi \tag{4.2}$$

with the following boundary conditions :

$$\begin{cases} \forall y \in [-1,+1] \quad \dfrac{\partial\psi}{\partial y}(0,y) = 0 \\ \forall x \geq 0 \quad \dfrac{\partial\psi}{\partial y}(x,-1) = 0, \quad \dfrac{\partial\psi}{\partial x}(x,-1) = 0, \quad \dfrac{\partial\psi}{\partial y}(x,1) = 0 \quad \dfrac{\partial\psi}{\partial x}(x,1) = 0 \end{cases} \tag{4.3}$$

As shown before, a possible choice for one stream function associated to the Taylor basic flow is $\bar{\psi} = x\sin(\pi y/2)$. Equation (4.2) represents then a linear equation with coefficients which are dependent on x and y and independent of t. Thus a general form for the unknown function $\psi(x,y,t)$ may be chosen with an exponential dependence with respect to t (normal mode in t) :

$$\psi(x,y,t) = e^{-i\omega t}\check{\psi}(x,y)$$

Equation (4.2) becomes then :

$$-i\omega\Delta\check{\psi} + \frac{\pi x}{2}\cos\frac{\pi y}{2}\frac{\partial}{\partial x}\Delta\check{\psi} - \frac{\pi^2}{4}\sin\frac{\pi y}{2}\frac{\partial\check{\psi}}{\partial y} - \sin\frac{\pi y}{2}\frac{\partial}{\partial y}\Delta\check{\psi} + \frac{\pi^3 x}{8}\cos\frac{\pi y}{2}\frac{\partial\check{\psi}}{\partial x} = \frac{1}{\mathcal{R}}\Delta\Delta\check{\psi}$$

whereas the associated boundary equations remain the same as (4.3), with $\breve{\psi}$ instead of ψ. A possible solution could be to solve directly the stability problem given by the previous homogeneous partial differential equation. Such problems are currently investigated by some researchers (in case of the stability of a recirculating zone, a vortex, the boundary layer in the vicinity of the attachment line etc.) but there is a strong difficulty with the treatment of the boundary conditions. The proposed solution is to search $\breve{\psi}$ in the form :

$$\breve{\psi} = x^{\lambda}\hat{\psi}(y)$$

leading hence to ordinary differential equations (like with the normal mode) and avoiding therefore the difficulty with the boundary conditions. The idea with this mathematical form is to define a phase velocity, which is then uniformly accelerated with x, as is the basic Taylor flow, whereas with the normal mode, the phase velocity does not depend on x. With this form, equation (4.2) writes :

$$\begin{aligned} 0 = & -\frac{1}{\mathcal{R}}D^4\hat{\psi} - i\omega D^2\hat{\psi} + \left[\frac{\lambda\pi}{2}\cos\frac{\pi y}{2} - \sin\frac{\pi y}{2}.D\right]\left(D^2\hat{\psi} + \frac{\pi^2}{4}\hat{\psi}\right) \\ & + \frac{1}{x^2}\left[-\frac{2}{\mathcal{R}}D^2 - i\omega + \frac{\pi}{2}\cos\frac{\pi y}{2}(\lambda - 2) - \sin\frac{\pi y}{2}.D\right]\lambda(\lambda-1)\hat{\psi} \\ & - \frac{1}{x^4}\frac{1}{\mathcal{R}}\lambda(\lambda-1)(\lambda-2)(\lambda-3)\hat{\psi} \end{aligned} \tag{4.4}$$

with D the differentiation operator with respect to y. As it is the case with the normal mode, this form does not satisfy exactly the equations, so that λ is not really independent of x. By using the so-called quasi-parallel approach, the value of λ is recalculated at each considered value of x.

The advantage of this form is clearly to define a zero-order approximation which is asymptotically valid for large values of x :

$$-\frac{1}{\mathcal{R}}D^4\hat{\psi} - i\omega D^2\hat{\psi} + \left[\frac{\lambda\pi}{2}\cos\frac{\pi y}{2} - \sin\frac{\pi y}{2}.D\right]\left(D^2\hat{\psi} + \frac{\pi^2}{4}\hat{\psi}\right) = 0 \tag{4.5}$$

On the other hand, let us return to the OSE and NNP approaches (obtained with the term $\exp(i\alpha x)$) for which, as proposed by J. Griffond, we define :

$$\lambda = ix\alpha$$

Then, the OSE approach gives :

$$-\frac{1}{\mathcal{R}}D^4\hat{\psi} - i\omega D^2\hat{\psi} + \frac{\lambda\pi}{2}\cos\frac{\pi y}{2}\left(D^2\hat{\psi} + \frac{\pi^2}{4}\hat{\psi}\right) + \frac{1}{x^2}\left[-\frac{2\lambda}{\mathcal{R}}D^2\hat{\psi} + \frac{\lambda^3\pi}{2}\cos\frac{\pi y}{2}\hat{\psi}\right] - \frac{1}{x^4}\frac{\lambda^4}{\mathcal{R}}\hat{\psi} = 0$$

whereas the NNP approach leads to :

$$\begin{aligned} 0 = & -\frac{1}{\mathcal{R}}D^4\hat{\psi} - i\omega D^2\hat{\psi} + \left[\frac{\lambda\pi}{2}\cos\frac{\pi y}{2} - \sin\frac{\pi y}{2}.D\right]\left(D^2\hat{\psi} + \frac{\pi^2}{4}\hat{\psi}\right) \\ & + \frac{1}{x^2}\left[-\frac{2\lambda^2}{\mathcal{R}}D^2\hat{\psi} + \left(\frac{\lambda\pi}{2}\cos\frac{\pi y}{2} - \sin\frac{\pi y}{2}.D\right)\lambda^2\hat{\psi}\right] - \frac{1}{x^4}\frac{\lambda^4}{\mathcal{R}}\hat{\psi} \end{aligned}$$

These equations show that for large values of x, the leading order (4.5) of (4.4) coincides exactly with the leading order of the NNP approach and NOT with the OSE approach. The inconsistent approach remains inconsistent obviously but is now justified (its leading order terms) for large values of x. Finally some comparisons between direct simulations (by using the code SIERRA developed by F. Vuillot, see [30]) and stability computations show a better agreement with (4.4) than with the NNP, see [24].

4.2 Physical assumptions

In addition to the assumption of a normal mode, there are several other aspects which have been neglected in the presentation given before. However, the effects of :

- compressibility,
- real geometry,
- presence of an acoustic mode,
- regression of the boundary wall

have been found to be nearly completely negligible. The intrinsic instability described before seems to be very robust.

The last point related to the linear stability theory, which appears to be important in the computations, see [31], concerns the effects of the presence of particles, especially of reactive particles. A first attempt in that direction has been achieved by taking into account non reactive particles. A first interesting result of [32] is that the particles may destabilise the flow, as it is illustrated in figure 4.4. This effect may be attributed to the appearing augmentation of the Reynolds number due to the augmentation of the density thanks to the particles.

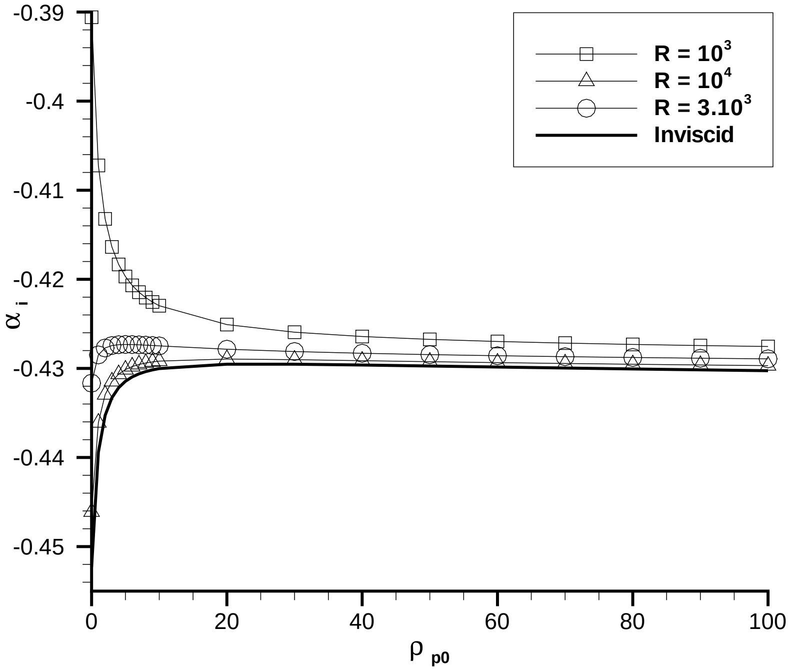

Figure 4.4: Evolution of the growth rate α_i as function of the density of the injected particles at the wall. The injection velocity of the particles is the same as the one of the fluid, the Stokes number is 10^{-3}, and $x = 10$, $\omega = 30$.

In addition to this two-phase flow effect, there is of course the linear assumption. But nonlinear mechanisms induced by instability are neither very easy nor very common. This could be another lecture ! See the thesis of J. Griffond [9] for detailed nonlinear analysis.

Conclusion

Undoubtedly, an intrinsic instability exists in the flow induced by wall injection. A linear stability theory can be carried out, even if it presents some difficulties (mainly from the theoretical point of view) in relation with the non parallel characteristics of the considered mean flow. At least in the plane geometry, the experimental results confirm the predictions based on the linear stability theory. However in practice, the intrinsic perturbation cannot grow infinitely in x, as it could be according to the linear stability results. From flow visualisations performed in VECLA, we know that large structures are emitted somewhere, they are associated to fluctuations of large amplitude and are thus not compatible with a small perturbation approach leading to the linear theory. The perturbations grow in x, according to the linear instability mechanism and then become fully non linear. Moreover, for some configurations the experimental results of VECLA do not seem to exhibit any instability feature. Among these results, there is the resonance on an acoustic mode of large amplitude which is of course the most important configuration in practice.

Where does this resonance phenomenon come from ? Does the stability play any role ?

In order to try to give some answers to these questions, let us summarise the main ideas (coming from the experimental results, direct simulations and nonlinear stability theories) obtained at the end of the PhD of J. Griffond. The key point is the dimensional value of the abscissa of the motor exit section x_s^*. It seems that the abscissa related to the instability mechanisms (location of the iso-n factor curves, location of the large structure emission) are mainly constant in term of dimensionless values, with the reference scale for the distance being the radius of the fluid h. But for a real motor, only x_s^* remains constant, the value of h grows continuously thanks to the regression of the injecting wall due to the combustion.

The proposed scenario is then the following one :

- At the beginning, h is small. In that case, the flow becomes turbulent somewhere in the duct, the large structures which are emitted upstream in the laminar zone are dissipated by the turbulence, so that there is no coherent (i.e. quasi periodic in time) structure which passes through the exit section. Nothing happens with respect to the cavity modes.
- Later, h becomes larger, the transition to turbulence moves downstream and at a given time, the turbulence zone is not sufficient to dissipate enough the large emitted structures. The frequency associated to this emission corresponds more or less to the one of the largest amplitude of the eigenmode at the abscissa from which nonlinear phenomena start to operate. At each time that a structure passes the throat (exit section), there is an emission of a reflecting pressure wave (it has been measured in the cold gas facilities). This wave arrives at the front wall and there is another reflecting wave, but now in the downstream direction. This wave may reasonably

excite the intrinsic instability mode (by the so-called receptivity mechanism) and mainly the one corresponding to its frequency. This mode is then fully favoured : it is an intrinsically amplified mode and it starts with a larger and larger amplitude due to the reflecting waves. Rapidly only one mode comes up. Then, at least in the VECLA and VALDO facilities, there are two cases : either the dominant frequency corresponds to the one of a cavity mode or not. The frequency obtained by the instability and the reflecting waves strongly depends on the injection velocity whereas the cavity frequencies are obviously mainly independent of this injection velocity. In the second case, the reflecting waves remain linear and the physics remains governed by the instability mechanism. In the first case, the amplitudes are very large and it may be guessed that the instability plays a role only in the transient which leads to the excitation of the cavity mode.

- Finally when h is large, the emission of the large structure does not occur any more in the booster, it moved downstream, only small fluctuations (the intrinsic instability modes themselves) remain and do not provide enough energy for creating reflected pressure waves.

This scenario needs of course additional confirmations but it is fully consistent with the experiment, the numerical simulations and the investigated nonlinear stability approaches.

Acknowledgement

This work has been included in a large research program named ASSM (Aerodynamics of Solid Segmented Motors) which was supported by CNES (Centre National d'Etudes Spatial) and was coordinated by ONERA (Office National d'Etudes et de Recherches Aérospatiales). The first author of the present course would also like to really thank P. Kuentzmann, F. Vuillot, G. Avalon for the very valuable discussions and advices.

Bibliography

[1] Lupoglazoff N. and Vuillot F. Parietal vortex shedding as a cause of instability for long solid propellant motors. numerical simulations and comparisons with firing tests. aiaa 96-0761. In *34th Aerospace Sciences Meeting and Exhibit.* AIAA, 15-18 janvier Reno, Nevada 1996.

[2] G. Avalon. Caractérisation des phénomènes liés à l'instabilité naturelle de l'écoulement dans le montage VECLA - Etude des conditions permettant de réaliser l'accrochage acoustique. Rapport final CNES 90/6133EY, ONERA, juillet 1997.

[3] Couton D., Plourde F., and Doan-Kim S. Cold gas simulation of a solid propellant rocket motor. *AIAA Journal*, 34:1462–1464, 1996.

[4] Avalon G., Ugurtas B., Grisch F., and Bresson A. Numerical computations and visualizations tests of the flow in a cold gas simulation with characterization of a parietal vortex-shedding. In *36th Joint Propulsion Conference and Exhibit, AIAA/ASME/ASEE, AIAA 2000-3387*, Huntsville, Alabama, 16-19 July 2000.

[5] Dunlap R., Blackner A., Waugh R., Brown R., and Willoughby P. Internal flow field studies in a simulated cylindrical port rocket chamber. *J. Propulsion*, 6, 1990.

[6] J. Anthoine. *Experimental and numerical study of aeroacoustic phenomena in large solid propellant motors.* PhD thesis, Université libre, Bruxelles, October 2000.

[7] V.N. Varapaev and V.I. Yagodkin. Flow stability in a channel with porous wall. *Izv. AN SSSR. Mekhanika Zhidkosi i Gaza.*, vol. 4, No 5, 1969.

[8] J. Griffond. Stabilité linéaire dans un conduit à parois débitantes. Effet de la régression de la paroi. Technical report, Rapport de DEA, ENSTA et Univ. P. et M. Curie, septembre 1998.

[9] J. Griffond. *Instabilité linéaire et non linéaire en conduit à parois débitantes.* PhD thesis, ENSAE, Toulouse, 21-Sept. 2001.

[10] Berman A. Laminar flow in channels with porous walls. *J. of applied Physics*, 24(9), september 1953.

[11] G. I. Taylor. Fluid flow in regions bounded by porous surfaces. *Proc. of the Royal Soc. Series A, London*, 234(1199):456–475, 1956.

[12] J. Ph. Pineau. Stabilité linéaire d'un écoulement dans un conduit cylindrique à paroi débitante. Rapport de DEA, CERT-ONERA, septembre 1997.

[13] P.G. Drazin and W. Reid. *Hydrodynamic stability.* Cambridge University, 1985.

[14] L. M. Mack. Boundary layer linear stability theory. *Special course on stability and transition of laminar flow*, 709, 1984.

[15] M. Gaster. A note on the relation between temporally increasing and spatially increasing disturbances in hydrodynamic stability. *J. of Fluid Mech.*, 14:222–224, 1962.

[16] J. Griffond, G. Casalis, and J. Ph. Pineau. Spatial instability of flow in a semiinfinite cylinder with fluid injection through its porous walls. *European Journal of Mechanics, B/Fluids*, 19, issue 1, Janvier 2000.

[17] M. Gaster. On the effect of boundary layer growth on flow instability. *J. of Fluid Mech.*, 66, 1974.

[18] D. Arnal, M. Habiballah, and E. Coustols. Théorie de l'instabilité laminaire et critères de transition en écoulement bi et tridimensionel. *La Recherche Aérospatiale*, 2, Mars - Avril 1984.

[19] G. Casalis, G. Avalon, and J. Ph. Pineau. Spatial instability of planar channel flow with fluid injection through porous walls. *Physics of Fluid*, 10(10), October 1998.

[20] G. Casalis and F. Charru. *Instabilités hydrodynamiques.* Cours du D.E.A. de mécanique des fluides de Toulouse, 1995.

[21] S. Hein, A. Hanifi, and G. Casalis. Nonlinear transition prediction. In *European Congress on Computational Methods in Applied Sciences and Engineering, ECCOMAS*, Barcelona, 11-14 september 2000.

[22] Th. Feraille. Phd, in preparation.

[23] Lee Y. and Beddini R. Acoustically-induced turbulent transition in solid propellant rocket chamber flowfields. In *35th AIAA/ASME/ASEE Joint Propulsion Conference and Exhibit, AIAA-99-2508*, Los Angeles, California, 20-24 June 1999.

[24] J. Griffond and G. Casalis. On the dependence on the formulation of some nonparallel stability approaches applied to the taylor flow. *Physics of Fluids*, 12(2), February 2000.

[25] C.M. Bender and S.A. Orszag. *Advanced mathematical methods for scientists and engineers.* McGraw-Hill, 1981.

[26] G. Casalis. *Méthodes mathématiques pour la mécanique.* Cours SUPAERO, 2000.

[27] Bridges T.J. and Morris P.J. Boundary layer stability calculations. *Physics of Fluids*, 30, november 1987.

[28] Th. Herbert and F. P. Bertolotti. Stability analysis of non-parallel boundary layers. *Bull. Am. Phys. Soc.*, 32, 1987.

[29] Ch. Airiau and G. Casalis. Stabilité linéaire de la couche limite par un système d'équations parabolique. *La Recherche Aérospatiale*, 5, Septembre-Octobre 1993.

[30] Vuillot F. Numerical computations of acoustic boundary layers in large solid propellant space booster. In *29th Aerospace Sciences Meeting*. AIAA 91-0206, Reno, Nevada, January 1991.

[31] Lupoglazoff N., Vuillot F., Dupays J., and Fabignon Y. Numerical simulations of the unsteady flow inside Ariane 5 P230 SRM booster with burning aluminium particles. In *2nd European Conference on Launcher Technology, Space Solid Propulsion*, Roma, 21-24 november 2000.

[32] Féraille T. and Casalis G. Particles effects on solid propellant motors flow stability. In *38th AIAA/ASME/SAE/ASEE Joint Propulsion Conference & Exhibit*, Indianapoli, Indiana, United States, 7-10, July 2002.

[33] Canuto C., Hussaini M., Quarteroni A., and Zang T. *Spectral methods in fluid dynamics.* Springer, 1988.

[34] M.R. Khorrami M.R. Malik R.L. Ash. Application of spectral collocation techniques to the th stability of swirling flows. *J. Comput. Physics*, vol. 81:pp. 206–229, 1989.

ANNEX : Spectral collocation method for eigenvalue problem

Description of the method

Several methods may be used for solving an eigenvalue problem or more generally any differential equations system. In the case of the plane Taylor flow, expressed in terms of stream function, equation (2.9), the simplest method is probably the spectral collocation method. In this annex, only a short view of it is given, more details together with other methods can be found in [33], an application of the spectral collocation technique in a particular stability problem is described in [34].

The goal is hence to solve the differential problem constituted by equation (2.9) and boundary conditions (2.10). The variable y varies in $[-1,+1]$. Some definitions are necessary, let be first T_n the n^{th} Chebychev's polynomial of degree n. Then, an integer N is assumed to be chosen, it characterises the chosen refinement for solving the differential problem, as it will be explained just below. Let be :

$$\xi_j = \cos\left(\frac{\pi j}{N}\right) \qquad j = 0, \ldots, N$$

$N+1$ points, which are called the ones of “Gauss-Lobatto”. The unknown amplitude function, which will be noted ψ in this annex, is approximated by the polynomial :

$$\psi(\xi) = \sum_{j=0}^{N} \lambda_j(\xi)\psi(\xi_j)$$

where λ stands for

$$\lambda_j(\xi) = \left(\frac{1-\xi_j^2}{\xi-\xi_j}\right)(-1)^{j+1}\frac{T'_N(\xi)}{N^2 c_j}$$

with T'_N the derivative of the N^{th} Chebychev's polynomial. The $N+1$ discrete values

$$\psi_j = \psi(\xi_j)$$

are explicitly the unknown of the (discretised) problem. This is the reason why N describes the used accuracy for computing the unknown. As ψ is a solution of differential problem, we have now to link between the derivative ψ' and the function ψ itself. For this purpose, let be :

$$\begin{aligned} E_{jk} &= \frac{c_j}{c_k}\frac{(-1)^{k+j}}{\xi_j-\xi_k} && j \neq k \\ E_{jj} &= -\frac{\xi_j}{2(1-\xi_j^2)} && j = 1, \ldots, N-1 \\ E_{00} &= -E_{NN} = \frac{2N^2+1}{6} \end{aligned}$$

defining a square matrix E with the coefficients c_j given by :

$$c_0 = c_N = 2 \qquad c_j = 1 \qquad j = 1, \ldots, N-1$$

Then, it can be proved that the derivative exactly corresponds for the discrete values to the matrix multiplication by E :

$$\frac{d\psi}{d\xi}(\xi_j) = \sum_{k=0}^{N} E_{jk}\psi_k$$

Typical stability code

Using the previous matrix multiplication as derivative operator leads to discretise the linearised stability equations into an algebraic problem for X the vector of the unknowns ψ_j. Then, there are usually two approaches, either the complete spectrum of the discretised problem is looked for or by a shooting method a unique value of the spectrum is looked for.

Spectrum. In this case, if the unknown is the complex number ω, the discretised problem is written under the form :

$$A.X = \omega B.X$$

with A and B two matrices coming from derivation and intervention of the mean flow. All the lines of the matrices correspond to the discretisation of the continuous equations at the collocation points, for example ordered from -1 up to +1. Then the four homogeneous boundary conditions are included by substituting the first line by the condition $\hat{\psi}(-1) = 0$, the second line by $\hat{\psi}'(-1) = 0$ and the two last lines in the same way (by the boundary conditions in $+1$). Thus the previous algebraic problem is replaced by :

$$\tilde{A}.X = \omega \tilde{B}.X$$

The last step consists in determining the eigenvalues ω by an appropriate method.

Shooting method. In this case, if the unknown is the complex number α, the discretised problem is written under the form :

$$A(\alpha).X = 0$$

As in the previous case, each lines expresses the continuous equation written in the corresponding collocation point. The idea in this case is as before to introduce the boundary conditions, but only three. In addition, a non homogenous one is introduced, for example a condition on the pressure (or the second derivative of $\hat{\psi}$). This non homogeneous condition acts as a normalisation condition. The previous problem is then replaced by :

$$\tilde{A}(\alpha).X = b$$

The next step consists in inverting $\tilde{A}(\alpha)$ and thus in determining X. Then, the omitted boundary condition is examined and in fact all the described procedure is included into a loop : α is searched until the omitted boundary condition is satisfied.

Code written in Matlab

A small program written using the commercial software Matlab is given below. The five routines are organised as described in figure 4.5. The main program is called “OrrSom”. The initialisation defines the collocation points and the matrix used for the derivation. Then, it is possible to compute the whole spectrum of the linearised operator, this is achieved in the routine “spectre”. Alternatively, the shooting method can be used, the initial guess is given in the main program, the routine “balai” defines possible parametric computations (by varying regularly one parameter among the Reynolds number, the frequency and the abscissa). This routine uses the one named “Newton” whose goal is to determine the eigenvalue by a standard Newton iterative procedure.

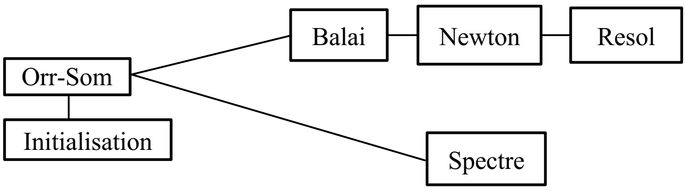

Figure 4.5: Representation of five Matlab routines for solving a stability problem with the spectral collocation method either with a shooting method (upper line “Balai - Newton - Resol”) or by determining the whole spectrum (lower line “Spectre”)

Each resolution of the stability equation called by “Newton” is performed thanks to the routine “Resol”.

Main program : orrsom.m

```
%
% Programme principal ORRSOM.m
%
% résolution du problème de stabilité linéaire
% pour l’écoulement dans un conduit plan à parois débitantes.
%   perturbation en forme de mode normal,
%   formulation en fonction de courant
%
%
global npol xi e id alpha omega reynolds csol type_calcul xloc;
%
% valeurs de départ
%2.48746e-001 9.70805e-001
reynolds = 1000;
xloc = 10;
omega = 31.6;
alpha = complex(4.0158,-0.373);
%
type_calcul = ’spectre’;
%
initialisation;
%
switch lower(type_calcul)
    case ’balai’
        balai;
    case ’spectre’
        spectre;
    otherwise
        disp(’Orr-Som, non implémenté’)
end
```

Subroutine : initialisation.m

```
%
% Sous-programme initialisation.m
%
% Initialisation dans la méthode de collocation spectrale
%  npol est le nombre de points de collocation
%  e    est la matrice de dérivation
%  id   est la matrice identité
%  xi   est le vecteur des points de collocation
%
global npol xi e c id;
%
% Préliminaires
%
npol = 100;
iaff = 0;
xi = zeros(npol,1); c = zeros(npol,1); id = zeros(npol,npol); e = zeros(npol,npol);
%
% Calcul du vecteur xi et du vecteur technique c
%
for j = 0:npol
    j1 = j+1;
    xi(j1,1) = cos(pi*j/npol); c(j1,1) = 1;
end
id = diag(c,0);
c(1,1)=2; c(npol+1,1)=2;
%
% Calcul de la matrice e
%
for j = 0:npol
    j1 = j+1;
    for k = 0:npol
        k1 = k+1;
        if (k~=j)
            e(j1,k1) = c(j1,1)*(-1)^(k+j)/(c(k1,1)*(xi(j1,1)-xi(k1,1)));
        else
            if (j~=0 & j~=npol)
                e(j1,j1) = -xi(j1,1)/(2*(1-xi(j1,1)*xi(j1,1)));
            end
        end
    end
end
e(1,1) = (2*npol*npol+1)/6; e(npol+1,npol+1) = -(2*npol*npol+1)/6;
```

Subroutine : spectre.m

```
%
```

```
% Sous-programme spectre.m
%
%  Détermination du spectre de l’opérateur d’Orr-Sommerfeld
%    on écrit le probleme sous la forme :
%          mat1.v = omega . mat2.v
%
% Paramètres
%
global npol xi e id alpha omega reynolds csol type_calcul vp xloc;
%
% initialisation
%
e2 = zeros(npol,npol); mat1 = zeros(npol,npol); mat2 = zeros(npol,npol) ;
ci = complex(0,1); e2=e*e ; e3=e2*e ;
%
% écoulement de base
%
u = pi*xloc*cos(pi*xi/2)/2; ddu = e2*u;
v = -sin(pi*xi/2); ddv = e2*v;
%
% remplissage des matrices mat1 et mat2
%
for i = 0:npol
    i1 = i+1;
    for j=0:npol
        j1=j+1;
        mat1(i1,j1) = -ci*alpha*(ddu(i1)+alpha*alpha*u(i1))*id(i1,j1);
        mat1(i1,j1) = mat1(i1,j1)+ci*alpha*u(i1)*e2(i1,j1);
        mat1(i1,j1) = mat1(i1,j1)-(alpha*alpha*v(i1)+ddv(i1))*e(i1,j1);
        mat1(i1,j1) = mat1(i1,j1) + v(i1)*e3(i1,j1);
    end
end
z1 =-1/reynolds; z2 = 2*alpha*alpha/reynolds ; z3 = -alpha.^4/reynolds;
mat1 = mat1 + z1*e2*e2 + z2*e2 + z3*id ;
mat2 = -ci*(alpha*alpha*id-e2) ;
%
% Conditions aux limites
%
for i = 0:npol
    i1=i+1;
    mat1(1,i1) = 0;mat2(1,i1) = 0;
    mat1(2,i1) = e(1,i1);mat2(2,i1) = 0;
    mat1(npol,i1) = e(npol+1,i1); mat2(npol,i1) = 0;
    mat1(npol+1,i1) = 0; mat2(npol+1,i1) = 0;
end
mat1(npol+1,npol+1) = 1; mat1(1,1) = 1;
%
```

```
% calcul des valeurs propres (généralisées)
%
bmat = eye(size(mat1));
l = eig(mat1,mat2);
%
% représentation graphique
%
plot(real(l),imag(l),'ob','MarkerSize',6,'MarkerFaceColor','b')
axis([0 100 -10 5])
```

Subroutine : balai.m

```
%
% Sous-programme balai.m
%
% calcul de valeurs propres avec Newton par variation de l'un des paramètres
%
% Ce paramètre peut etre :
%   le nombre de Reynolds
%   la position en abscisse
%   la fréquence
%
%
global alpha omega reynolds xloc;
%
% Valeurs initiales pour la variation
%
type_balai = 'reynolds';
nparam = 1; dparam = 100;
%
% Lecture du fichier où sont écrites les valeurs précédentes
%
fid = fopen('C:\GREG\ONERA\SPADA\StabMatlab\varirey.txt','a+');
%
[vect,count] = fscanf(fid,'%f %f %e %e %e',inf);
nligne = count/5; indice = 5*(nligne-1);
reynolds = vect(indice+1); xloc = vect(indice+2);
omega = vect(indice+3);
alpha = complex(vect(indice+4),vect(indice+5));
%
% Valeurs pour démarrer le calcul
%
alphainit = alpha; omegainit = omega;
reynoldsinit = reynolds; xlocinit = xloc;
%
% Variation suivant le paramètre choisi
%
switch lower(type_balai)
```

```
    case 'frequence'
        domega = dparam; dreynolds = 0; dxloc = 0;
    case 'abscisse'
        domega = 0; dreynolds = 0; dxloc = dparam;
    case 'reynolds'
        domega = 0; dreynolds = dparam; dxloc = 0;
    otherwise
        disp('non implémenté (ou erreur) dans balai')
end
%
%  Boucle pour la variation du paramètre choisi
%
for iparam = 1:nparam
    omega    = omegainit    + (iparam-1)*domega;
    reynolds = reynoldsinit + (iparam-1)*dreynolds;
    xloc     = xlocinit     + (iparam-1)*dxloc;
    %
    % Estimation des valeurs initiales
    %
    switch lower(iparam)
    case 1
        alpha = alphainit;
    case 2
        alpha = alpha1;
    case 3
        alpha = 2*alpha2 - alpha1;
    otherwise
        alpha = 3*(alpha3-alpha2) + alpha1;
    end
    %
    % Appel à la convergence, méthode de Newton
    %
    newton;
    %
    % Stockage des au plus 3 dernières valeurs convergées
    %
    switch lower(iparam)
    case 1
        alpha1 = alpha;
    case 2
        alpha2 = alpha;
    case 3
        alpha3 = alpha;
    otherwise
        alpha1=alpha2; alpha2=alpha3; alpha3=alpha;
    end
    %
    % Affichage écran des résultats
    %
    fprintf('iparam = %d, R = %0.1f, X = %0.1f, w = %0.5e, ar = %0.5e, ai = %0.5e\n\n\n',...
        iparam,reynolds,xloc,omega,real(alpha),imag(alpha))
    %
    % Ecriture sur fichier des résultats
    %
    fprintf('\n')
    fprintf(fid,'%0.1f %0.1f %0.5e %0.5e %0.5e \n ',...
        reynolds,xloc,omega,real(alpha),imag(alpha));
end
%
status = fclose(fid);
```

Subroutine : newton.m

```
%
% Sous-programme Newton.m
%
% Méthode de Newton complexe pour
%  résoudre csol = 0, alpha est l'inconnue complexe
%
global npol xi e id alpha omega reynolds csol type_calcul;
%
% Initialisation Newton
%
dval = 1E-4;
err = 1;
it = 0;
alphan = alpha ;
%
% Méthode de Newton (utilisation des relations de Cauchy)
%
while (err > 1E-08 & it < 10)
   it = it + 1;
   alpha = alphan;
   resol; csol0 = csol ;
   alpha = alphan + dval;
   resol; csolm = csol;
   dcsol = (csolm-csol0)/dval; cor = csol0/dcsol;
   err = abs(cor)/abs(alphan);
   alphan = alphan - cor;
end
if (err > 1E-06)
    disp('problème Newton')
    break
end
```

Subroutine : resol.m

```
%
% Sous-programme resol.
%
% On ecrit Orr-Sommerfeld sous la forme mat.X = b
%
%    e2  : matrice de dérivée seconde e2 = e*e
%
global npol xi e id c alpha omega reynolds csol xloc;
%
% initialisation
%
b = zeros(npol,1); e2 = zeros(npol,npol); mat = zeros(npol,npol);
e3 = zeros(npol,npol);
ci = complex(0,1); e2=e*e; e3=e2*e;
%
% écoulement de base
%
u = pi*xloc*cos(pi*xi/2)/2; ddu = e2*u;
v = -sin(pi*xi/2); ddv = e2*v;
%
% remplissage de la matrice mat
%
for i = 0:npol
    i1 = i+1;
    for j=0:npol
        j1=j+1;
        mat(i1,j1) = -ci*alpha*(ddu(i1)+alpha*alpha*u(i1))*id(i1,j1);
        mat(i1,j1) = mat(i1,j1)+ci*alpha*u(i1)*e2(i1,j1);
        mat(i1,j1) = mat(i1,j1)-(alpha*alpha*v(i1)+ddv(i1))*e(i1,j1);
        mat(i1,j1) = mat(i1,j1) + v(i1)*e3(i1,j1);
        mat(i1,j1) = mat(i1,j1) -ci*omega*e2(i1,j1) ;
    end
end
z1 =-1/reynolds; z2 = 2*alpha*alpha/reynolds ;
z3 = -alpha.^4/reynolds + ci*omega*alpha*alpha ;
mat = mat + z1*e2*e2 + z2*e2 + z3*id ;
%
% conditions aux limites
% on écrit psi"(1) = 1, psi'(1) = 0, psi'(-1) = 0, psi(-1) = 0
%
for i = 0:npol
    i1=i+1;
    mat(1,i1) = e2(1, i1);
    mat(2,i1) = e(1,i1);
    mat(npol,i1) = e(npol+1,i1);
    mat(npol+1,i1) = 0;
    b(i1) = 0;
end
mat(npol+1,npol+1) = 1; b(1) = 1;
%
% inversion
%
sol_v = mat\b ;
%
% si iaff=0, c'est Newton sur v(1), sinon affichage de la fonction propre
%
iaff = 0;
if (iaff == 0)
    csol = sol_v(1);
else
    sol_dv = e*sol_v;
    plot(xi,abs(sol_v),xi,abs(sol_dv),'LineWidth',2)
    set(gca,'DefaulttextFontName','Times New Roman');set(0,'DefaulttextFontSize',14);
    xlabel('{\it y}','FontName','Times New Roman','FontSize',16);
    ylabel('{\it u,v}','FontName','Times New Roman','FontSize',16);
    legend('u','v',0);
end
```